To the Graduate Council:

I am submitting herewith a dissertation written by L. Montgomery Smith entitled "A Unified Study of the Effects of Aberrations in Focused Laser Beams." I have examined the final copy of this dissertation for form and content and recommend that it be accepted in partial fulfillment of the requirements for the degree of Doctor of Philosophy, with a major in Electrical Engineering.

Igor Alexeff

Igor Alexeff, Major Professor

We have read this dissertation and recommend its acceptance:

Dennis Keefer

Bruce Bomar

M. J. Roberts

Fred Hoffman

Accepted for the Council:

C W Minkel

Vice Provost
and Dean of the Graduate School

A UNIFIED STUDY OF THE EFFECTS OF ABERRATIONS IN FOCUSED LASER BEAMS

A Dissertation

Presented for the

Doctor of Philosophy

Degree

The University of Tennessee, Knoxville

L. Montgomery Smith

December 1988

ACKNOWLEDGEMENTS

The author would like to express his sincere appreciation to several individuals who assisted in the efforts presented in this dissertation. Special thanks are extended to Dr. Dennis Keefer, who supervised the day-to-day activities in guiding the research, and to Dr. Igor Alexeff, who served as the major professor on the doctoral committee. The efforts and advice of Dr. Bruce Bomar are greatly appreciated, as are the efforts of the remaining committee members, Dr. Graham Hoffman and Dr. Michael Roberts.

Further appreciation is given to Mr. Jim White, whose assistance with digital hardware aided both the theoretical and experimental aspects of this effort, and to Mr. Newton Wright for his help in the laboratory. Mr. Boyd Stubblefield developed and printed the photographs contained in the figures. Correspondence with Dr. Roland Anderson of The University of Florida proved beneficial at the beginning of the research. Finally, the cooperation and encouragement of Mr. Jim Few and the other members of the Center for Laser Applications staff are respectfully acknowledged.

This work was supported in part by the Air Force Office of Scientific Research under Grant AFOSR-86-0317 and by the Center for Laser Applications through funding provided by the Tennessee Higher Education Commission.

ABSTRACT

A theoretical and experimental investigation was conducted of the intensity distribution of radiation in the focal region for a laser beam focused by a lens. A Fourier optics approach was taken to derive the integral equations expressing the focused field resulting from a general amplitude and phase field distribution incident on a spherical surface lens. The effects of aberrations resulting from the lens as well as the propagation properties of the electromagnetic radiation were included, and these effects were expressed explicitly in terms of the optical system parameters. The lens effects were taken into account using a second-order series expansion derived from the thin lens approximation. Two approaches, one based upon the two-dimensional convolution integral and the other upon the two-dimensional Fourier transform integral, were derived to calculate the field as it propagates to focus. These equations were implemented on a digital computer to calculate transverse and meridional plane intensity distributions. Calculated data were displayed in image format for visual interpretation.

Experimental verification of the theory was performed for a plano-convex lens focusing a helium-neon laser beam. Data were acquired in image format with a digital image processor, and images were constructed of the meridional plane intensity distributions for several incident beam profiles. Strong agreement was found to exist both quantitatively and qualitatively between calculated and experimental results.

TABLE OF CONTENTS

LIST OF FIGURES

I. INTRODUCTION

In many applications, a laser beam is focused to produce a small region of high light intensity. In laser sustained plasmas, focusing of the beam is necessary to produce sufficiently high intensities so that the plasma is stable. Laser induced fluorescence also frequently employs a focused beam in order to obtain adequate signal power from a few fluorescing molecules within a small probe volume. In material processing methods such as welding, cutting and drilling, a focused laser is used to melt or vaporize a hardened metal or ceramic part. Other areas such as laser fusion and laser induced chemistry also make use of focused laser beams.

In all of these applications, a complete understanding of the physical processes involved relies upon knowledge of the intensity of the light near the focal point of the lens. This intensity distribution in the focal region, however, is complicated by the effects of diffraction due to the finite size of the lens, the amplitude and phase profile of the incident beam, and aberrations arising from the lens and propagation properties of light. Geometrical ray-tracing methods are useful for analyzing the major phenomena associated with the behavior of light, but they do not consider the wave nature of light, and hence fail when the spatial extent of the region of interest is within approximately two orders of magnitude of the wavelength. Diffraction theory must be used for a more accurate analysis on a microscopic scale.

The problem can thus be stated verbally in the following manner: given a known complex representation of the field describing the laser beam incident on a lens with known specifications, what is the distribution of light intensity in the small region behind the lens called focus? The description of the intensity should be on as fine a scale as possible and should include the effects of the overall focusing process, interference, diffraction, and aberrations.

In this effort, a Fourier optics approach was taken to study the intensity distribution within the focal region resulting from a monochromatic laser beam with arbitrary amplitude and phase variations incident upon a spherical surface lens. Emphasis was placed on including the effects of aberrations in the analysis, since aberrations, particularly spherical aberration, can significantly affect the intensity pattern at focus for small F number focusing systems, like those employed in many of the applications previously discussed.

The approach that was taken was divided into two parts. The first part was the theoretical analysis in which Fourier optics theory was used to model mathematically the effects of the focusing lens and the propagation of the light to the focal region. The resulting integral equations were then discretized and implemented using digital signal processing algorithms on a digital computer, and the calculated results were displayed in image format on a digital image processor for visual interpretation. The second part was the experimental verification of the calculated results. Optical intensity data in this part was taken with the aid of the digital image processor in the same format and with the same fields of view as the calculated intensity results, and so could be directly compared visually. For the particular beam profiles studied, the calculated and experimental results show strong agreement.

The organization of this dissertation is as follows. In Chapter II, some of the previous work in the diffraction theory of aberrations is discussed. The notation and the mathematical statement of the problem are introduced in Chapter III. Because of the importance of the early groundwork laid by Nijboer and Zernike, a short monograph of his approach is given in Chapter IV. In Chapter V, the Fourier optics theory is presented, and two approaches are derived to calculate the focused light intensity distribution. The discretization of the integral equations derived in Chapter V is presented in Chapter VI, and a few calculated results are presented in Chapter VII. In Chapter VIII, some of the limitations of the approaches taken here and some of the shortcomings of the assumptions are discussed. The experimental technique used to verify the theoretical work is described in Chapter IX, and the experimentally acquired results are presented in Chapter X. Finally, Chapter XI concludes the dissertation with a short discussion.

II. PREVIOUS WORK

Although the earliest work in the diffraction theory of aberrations can be traced to Rayleigh in 1879 [1], * it was not until the 1940's that Nijboer and Zernike [2]-[4] developed the diffraction theory of image formation in the presence of aberrations that has widespread application even today. Restricting their attention to uniform amplitude illumination in the circular exit pupil of a coherent optical system, they accounted for the effects of aberrations by inserting an additional phase term in the complex exponential of the diffraction integral. The phase was then expanded in a series of orthogonal polynomials, called the circle polynomials of Zernike, and the individual terms in the expansion were then classified as spherical aberration, coma, astigmatism, field curvature, or distortion according to their effects upon the output image. This approach allowed for simplification of the two-dimensional diffraction integral into a descending series of one-dimensional integrals involving tabulated functions.

In 1948, Kingslake [5] and Nienhuis [6],[7] followed up the Nijboer-Zernike theory with some experimental work in which intensity patterns produced in the presence of primary aberrations were photographed in several transverse planes (planes orthogonal to the optical axis). Later, Maréchal [8] employed a mechanical integrator to perform calculations of the intensity distribution in the meridional plane (a plane containing the optical axis) for a uniform circular beam

* Numbers in brackets refer to similarly numbered references in the Bibliography.

focused in the presence of primary spherical aberration, and also of transverse plane intensity distributions for combined aberration effects. The theory and results of this early work are presented in Linfoot [9] and Born and Wolf [10].

While this approach formed a basis for the diffraction theory of aberrations, and was ingenious in light of the limited computing power of the day, it has its limitations. It considered only uniform amplitude illumination of a circular lens. It was computationally difficult, in general requiring an integrator constructed especially for the purpose. It did not express the aberrations explicitly in terms of the optical system parameters. And finally, the data display in terms of isophote contour plots (lines of equal intensity) was often confusing. As an example of this early work, Fig. 1 shows an isophote contour plot generated by Maréchal of the meridional plane intensity distribution in the presence of spherical aberration.

With renewed interest in this problem generated by the invention of the laser, others extended the results of this early work to non-uniform beam profiles [11],[12]. Lowenthal [13] and Sklar [14] studied the focusing of Gaussian and truncated Gaussian beams, respectively. Yoshida [15] considered a non-radially symmetric case by analyzing the focusing of off-axis uniform and Gaussian beams. Computational efficiency was not significantly improved in any of these schemes, however, and the circular symmetry of the input beam was necessary to the analysis in all cases. Data display, if attempted at all, never improved over isophote contour plots.

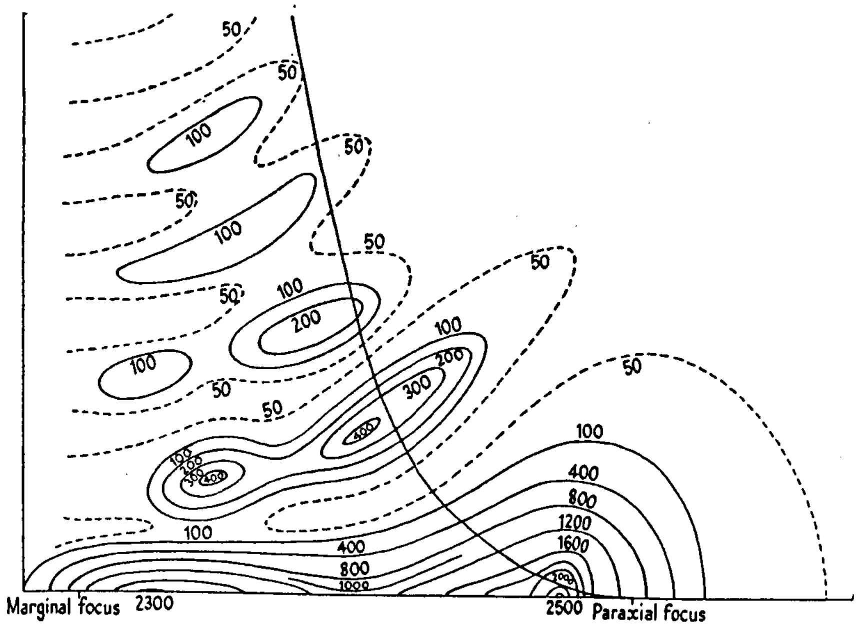

Fig. 1. Isophote contour plot of meridional plane intensity distribution for a focused uniform circular beam in the presence of primary spherical aberration. After Maréchal [8], reprinted in Linfoot [9].

Recently, Geary and Peterson [16] used a Fourier optics approach to derive a formulation for the focused intensity of a uniform plane wave. By expanding the phase shifting term in the thin lens approximation model and retaining terms to second order, they obtained an expression describing spherical aberration that was explicitly dependent upon the lens parameters. Other terms in the diffraction integral were retained only to first order, however, so the analysis appears incomplete. Also, the problem was formulated only for radially symmetric optical systems. Pursuant to their theoretical work, Geary and Peterson also performed an experimental investigation of focusing systems with spherical aberration [17].

In this work, they placed a fiber optic scanner in the focal region of a lens and obtained one-dimensional scans of focused beam intensity as a function of the radial coordinate in different transverse planes.

Work continues in this area. Li and Wolf have published a series of papers on the focal shift [18],[19]. They have shown that the peak on-axis intensity for a converging spherical wave passing through a circular aperture occurs before the geometrical focus. Their most recent contributions have included meridional plane isophote contour plots of the intensity distribution in the focal region for such cases [20],[21]. Still, the analysis is carried out only for uniform amplitude illumination of a circular aperture.

The work reported here was an effort to overcome some of the shortcomings and limitations associated with this earlier work. The theoretical work was formulated to accept any amplitude and phase distribution in the incident field, and to calculate the aberration effects explicitly as functions of the focusing lens parameters. Higher-order terms were retained in the diffraction integral to account for their effects on the output field. The resulting equations were then discretized for efficient computation using fast numerical algorithms available in digital array-processing hardware. By displaying calculated intensity distributions in image format, data interpretation was made easy. The experimental work also improved on earlier work by acquiring data in image format and in the meridional plane, which illustrates the focusing process quite effectively.

III. MATHEMATICAL STATEMENT OF THE PROBLEM

All previous discussion of the problem of focusing a laser beam has been verbal. In this chapter, the problem is formulated quantitatively in terms of scalar diffraction theory. The notation will follow closely that in the book by Goodman [22].

The propagation of light in most laboratory optical systems is either through free space, or at least through nonconducting dielectric media. While a complete description of the radiation requires specifying three components of the electric field and three components of the magnetic field as functions of spatial position (x, y, z) and time t, in many cases one component suffices to adequately characterize the radiation. Thus let $u(x, y, z; t)$ denote one scalar component of either the electric or the magnetic field. For laser radiation, the fields are nearly monochromatic, so that to a very close approximation, $u(x, y, z; t)$ can be written

$$u(x, y, z; t) = u(x, y, z) \cos\left[2\pi\nu t - \varphi(x, y, z)\right], \tag{1}$$

where $u(x, y, z)$ is the real field amplitude, ν is the frequency of the light, and $\varphi(x, y, z)$ is the phase of the field at the point (x, y, z). The analysis is simplified by working with the complex analytic function representation of the fields where the real field component is understood to be

$$u(x, y, z; t) = \mathrm{Re}\{U(x, y, z)e^{-j2\pi\nu t}\}. \tag{2}$$

In (2), the phase term has been absorbed into the complex amplitude function $U(x, y, z)$.

From Maxwell's equations, the field amplitude $U(x, y, z)$ can be shown to satisfy the time-independent Helmholtz equation [10],[22]

$$\nabla^2 U(x, y, z) + k^2 U(x, y, z) = 0, \tag{3}$$

where k is the propagation constant defined by $k = 2\pi/\lambda$, and λ is the wavelength of the radiation. Equation (3) serves as the fundamental starting point for the derivation of the Rayleigh-Sommerfeld diffraction integral, the mathematical relation that describes the propagation of light over any distance large as compared to the wavelength.

The derivation of the Rayleigh-Sommerfeld diffraction formula is rather long and involves Green's theorem along with judicious choices for the volume and surface of integration and a suitable Green's function. A complete derivation using the present notation can be found in [22, pp. 30-46]. For brevity, only the result is presented here. Let $U(x_1, y_1, z_1)$ be the field in the (x_1, y_1)-plane at the location on the z-axis where $z = z_1$, as shown in Fig. 2. The field $U(x_0, y_0, z_0)$ in the (x_0, y_0)-plane at $z = z_0$ is then given by

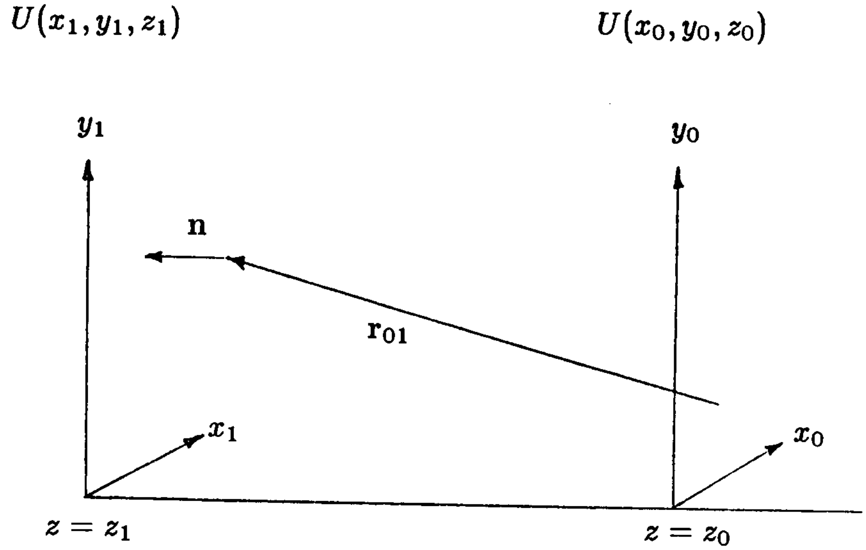

Fig. 2. Geometric configuration for Rayleigh-Sommerfeld diffraction integral.

$$U(x_0, y_0, z_0) = \frac{1}{j\lambda} \int_{-\infty}^{\infty} \int_{-\infty}^{\infty} U(x_1, y_1, z_1) \frac{\exp(jkr_{01})}{r_{01}} \cos(\mathbf{n}, \mathbf{r}_{01}) dx_1 dy_1, \quad (4)$$

where $\mathbf{r}_{01}$ is the vector from (x_0, y_0, z_0) to (x_1, y_1, z_1) and $\mathbf{n}$ is the outward unit normal to the (x_1, y_1)-plane. Clearly, the evaluation of (4) for arbitrary $U(x_1, y_1, z_1)$ is not a simple task.

At this point, the problem of beam focusing can be quantitatively stated. Let a lens be centered on the optical axis with its front surface located at $z = 0$, and its rear surface at $z = \Delta_o$, where Δ_o is the maximum thickness of the lens. Let $U(x, y, 0)$ denote the complex field amplitude incident on the lens. What is the effect of the lens that produces the transmitted field $U(x, y, \Delta_o)$ at the back surface of the lens, and how can the Rayleigh-Sommerfeld diffraction integral (4) be evaluated in order to calculate the field in the focal region $U(x_f, y_f, z_f)$ from the given $U(x, y, \Delta_o)$?

Conventional first-order scalar diffraction theory takes the following approach to this problem. First, the effect of the lens is based upon the thin lens approximation. In the thin lens approximation, the magnitude of the amplitude distribution is assumed not to change as the field propagates from the front to the back surface of the lens, except for the windowing introduced by the finite aperture size. The phase of the incident field, however, is altered as the field passes through the varying thickness of the lens material that has index of refraction n. Thus, the transmitted field is related to the incident field by the multiplicative relation

$$U(x, y, \Delta_o) = U(x, y, 0) P(x, y) \exp[jk\Delta_o] \exp[jk(n-1)\Delta(x, y)], \tag{5}$$

where $P(x, y)$ is the pupil function describing the lens aperture and $\Delta(x, y)$ is the thickness of the lens at the location (x, y).

For a spherical surface lens with a front surface radius of curvature R_1 and a rear surface radius of curvature R_2, the thickness is given by [22]

$$\Delta(x, y) = \Delta_o - R_1\left(1 - \sqrt{1 - \frac{x^2 + y^2}{R_1^2}}\right) + R_2\left(1 - \sqrt{1 - \frac{x^2 + y^2}{R_2^2}}\right). \tag{6}$$

The standard approach is to assume that the values of x and y remain sufficiently small over the lens aperture so that the square root expressions can be expanded in a Taylor's series and higher-order terms neglected. In this case, the thickness can be approximated by

$$\Delta(x,y) \cong \Delta_o - \frac{x^2+y^2}{2}\left(\frac{1}{R_1} - \frac{1}{R_2}\right). \tag{7}$$

Substitution of this term into (5), and use of the definition of the focal length of the lens

$$\frac{1}{f} \equiv (n-1)\left(\frac{1}{R_1} - \frac{1}{R_2}\right) \tag{8}$$

yields the relationship of the transmitted field to the incident field as approximately given by

$$U(x,y,\Delta_o) \cong U(x,y,0)P(x,y)\exp[jkn\Delta_o]\exp\left[-j\frac{\pi}{\lambda f}(x^2+y^2)\right]. \tag{9}$$

The phase term $\exp[jkn\Delta_o]$ is a complex constant that does not affect the spatial variation of the transmitted field and so will be dropped from the analysis in the future.

For the propagation of the transmitted field to the focal region, the conventional approach is to approximate the Rayleigh-Sommerfeld diffraction integral.

If the propagation distance from the rear surface of the lens to the (x_f, y_f)-plane defined by $z_p = |z_f - \Delta_o|$ is assumed to be large as compared to the physical extent of the field within the lens aperture, then over the area of integration, the obliquity factor $\cos(\mathbf{n}, \mathbf{r}_{01})$ remains approximately equal to unity, and in the denominator, the distance r_{01} approximately equals z_p. In the exponential term, the distance r_{01}, which is given exactly by

$$r_{01} = \sqrt{(x_f - x)^2 + (y_f - y)^2 + z_p^2}, \tag{11}$$

is expanded in a Taylor's series, and again, higher-order terms are neglected. The resulting expression for the field in the focal region is then given by

$$\begin{aligned} U(x_f, y_f, z_f) \cong & \frac{\exp[jkz_p]}{j\lambda z_p} \exp\left[j\frac{\pi}{\lambda z_p}(x_f^2 + y_f^2)\right] \int_{-\infty}^{\infty}\int_{-\infty}^{\infty} U(x, y, 0) P(x, y) \\ & \times \exp\left[j\frac{\pi}{\lambda}\left(\frac{1}{z_p} - \frac{1}{f}\right)(x^2 + y^2)\right] \exp\left[-j\frac{2\pi}{\lambda z_p}(xx_f + yy_f)\right] dxdy. \end{aligned} \tag{12}$$

Because the quantity of interest is the functional variation of the focused intensity given by $I(x_f, y_f, z_f) = |U(x_f, y_f, z_f)|^2$, the constants and phase terms multiplying the integral can be dropped from the analysis, and the mathematical symbol "$\sim$" is introduced to denote the relationship between the focused field and the integral expression that the theory predicts for it. Note that the symbol "$\sim$" is not used here to denote "approximately equal to" but rather means "aside from a multiplicative phase term, proportional to."

Clearly, errors can be introduced by the approximations made in deriving (12). And, although the approximations for the obliquity factor and the distance r_{01} in the denominator may not be valid in some cases, the omission of higher-order terms in the complex exponentials is usually the dominant factor that causes deviation from first-order diffraction theory. If the function $\Phi(x, y; x_f, y_f, z_f)$ is introduced to include these higher-order terms, then the expression for the focused field can be more accurately written as

$$U(x_f, y_f, z_f) \sim \frac{1}{z_p} \int_{-\infty}^{\infty} \int_{-\infty}^{\infty} U(x, y, 0) P(x, y) \exp[jk\Phi(x, y; x_f, y_f, z_f)]$$
$$\times \exp\left[j\frac{\pi}{\lambda}\left(\frac{1}{z_p} - \frac{1}{f}\right)(x^2 + y^2)\right] \exp\left[-j\frac{2\pi}{\lambda z_p}(xx_f + yy_f)\right] dxdy. \tag{13}$$

The effects that the additional phase term has on the focused field are called *aberrations.* The problem addressed in this dissertation is how to quantify these effects and include them in the calculation of the focused intensity distribution.

Note that the aberrations, as defined here, are introduced by both the lens and the propagation properties of the radiation. That is, not only does the spherical surface lens produce deviations in phase from the first-order approximation, but the behavior of the light as described by the Rayleigh-Sommerfeld diffraction formula also deviates slightly from the expression derived using the simplifying approximations previously described. Even with a so-called "ideal" aspheric lens, the calculation of the field as it propagates from the plane in the rear of the lens to planes in the focal region is complicated by additional terms in the complex exponential of the integral that make numerical evaluation difficult and affect the intensity distribution of the light. Because these phenomena are similar in their effects to those caused by the lens, they are also justifiably called aberrations.

In the following chapter, the classical Nijboer-Zernike approach to this problem is outlined. In Chapter V, the Fourier optics approach is presented in more detail. As will be seen, while the overall effects of a lens are well known, and the integral expression for the propagation of light is exactly formulated as given in (4), the calculation of the focused field is by no means trivial.

IV. THE NIJBOER-ZERNIKE APPROACH

The approach taken by Nijboer and Zernike to the diffraction theory of aberrations is a useful technique that has been followed not only by other earlier workers in the field [5]-[8], but also by more recent authors [11]-[15]. Because of its importance and utility to the field, it is worth repeating in light of the Fourier optics approach taken here. Strictly speaking, the problem addressed by Nijboer and Zernike is that of point imaging, however, it is easily extended to the case of focusing by assuming the object to be located on axis at infinity.

The analysis began by assuming the field $U(x, y, 0)$ to have constant complex amplitude over the exit pupil that is in turn assumed to be a circular aperture of radius a. The integral was then rewritten in terms of cylindrical coordinates defined by

$$x = a\rho\cos\theta, \qquad x_f = r\cos\psi$$

$$y = a\rho\sin\theta, \qquad y_f = r\sin\psi.$$

With this change of variables the focused field can be written

$$U(r,\psi,z_f) \sim \frac{1}{z_p}\int_0^{2\pi}\int_0^1 \exp[jk\Phi(\rho,\theta;r,\psi,z_f)] \times \exp\left[j\frac{\pi a^2}{\lambda}\left(\frac{1}{z_p}-\frac{1}{f}\right)\rho^2\right]\exp\left[-j\frac{2\pi a r\rho}{\lambda z_p}\cos(\theta-\psi)\right]\rho d\rho d\theta. \tag{14}$$

Note that the field and aberration term are written as functions of the cylindrical coordinates ρ, θ, r, ψ, and z_p.

Next, the region of interest was restricted to the region near the focus predicted by first-order theory, that is, where $r \cong 0$, and $z_p = |z_f - \Delta_o| \cong f$. Under this restriction, the term multiplying the integral is approximately constant and the aberration term is a function of ρ and θ only. In the second exponential, setting $z_p = f + \Delta z$, where $\Delta z \ll f$, results in the approximation

$$\frac{1}{z_p} - \frac{1}{f} \cong -\frac{\Delta z}{f^2}.$$

In the last exponential, z_p is simply approximated by f. The integral was then rewritten in terms of the optical coordinates

$$v = \frac{2\pi a}{\lambda f} r, \qquad \varsigma = \frac{2\pi a^2}{\lambda f^2} \Delta z$$

in the following form:

$$U(v, \psi, \varsigma) \sim \int_0^1 \int_0^{2\pi} \exp\left\{ j\left[k\Phi(\rho, \theta) - \frac{\varsigma \rho^2}{2} - v\rho \cos(\theta - \psi) \right] \right\} \rho d\rho d\theta. \qquad (15)$$

To evaluate this integral over the unit circle, Nijboer and Zernike expanded the aberration function in a series of orthogonal polynomials called the Zernike circle polynomials as

$$k\Phi(\rho,\theta) = \alpha_{00} + \frac{1}{\sqrt{2}}\sum_{n=2}^{\infty}\alpha_{n0}R_n^0(\rho) + \sum_{n=1}^{\infty}\sum_{m=1}^{\infty}\alpha_{nm}R_n^m(\rho)\cos(m\theta), \tag{16}$$

where $R_n^m(\rho)$ is a Zernike circle polynomial defined by

$$R_n^m(\rho) = \sum_{i=0}^{\frac{1}{2}(n-m)} (-1)^i \frac{(n-i)!}{i![\frac{1}{2}(n+m)-i]![\frac{1}{2}(n-m)-i]!}\rho^{n-2i}. \tag{17}$$

In this way, each aberration was described and quantified by the corresponding coefficient α_{nm} in the expansion (16). For example, primary spherical aberration was represented by $n = 4$ and $m = 0$, primary coma by $n = 3$ and $m = 1$, and primary astigmatism by $n = 2$ and $m = 2$. Other primary aberration terms, and the secondary aberration terms, are tabulated in [9] and [10].

From here, the approach taken was to consider each aberration separately. For a single aberration, the function $k\Phi(\rho,\theta)$ is equal to simply $\alpha_{nm}R_n^m(\rho)\cos(m\theta)$. Next, the well-known identity

$$\exp(jz\cos\phi) = J_0(z) + 2\sum_{p=1}^{\infty} j^p J_p(z)\cos(p\phi)$$

was applied separately to each of the two terms

$$\exp[-jv\rho\cos(\theta-\psi)], \qquad \exp[j\alpha_{nm}R_n^m(\rho)\cos(m\theta)],$$

where $J_p(.)$ denotes the p^{th}-order Bessel function. Multiplying the two series and integrating term by term over θ yields the following expression for the focused field:

$$
\begin{aligned}
U(v,\psi,\varsigma) \sim & \int_0^1 \exp\left[-j\frac{\varsigma\rho^2}{2}\right] J_0\left[\alpha_{nm}R_n^m(\rho)\right] J_0(v\rho)\rho d\rho \\
& + 2\sum_{p=1}^{\infty} j^{p(m-1)} \cos(pm\psi) \\
& \times \int_0^1 \exp\left[-j\frac{\varsigma\rho^2}{2}\right] J_p\left[\alpha_{nm}R_n^m(\rho)\right] J_{pm}(v\rho)\rho d\rho.
\end{aligned}
\tag{18}
$$

The final step in the manipulation of the equation was to expand each function $J_p[\alpha_{nm}R_n^m(\rho)]$ in its power series representation, and to rearrange terms into powers of $j\alpha_{nm}$. The focused field can then be written in the form

$$
U(v,\psi,\varsigma) \sim \sum_{p=0}^{\infty} (j\alpha_{nm})^p U_p(v,\psi,\varsigma), \tag{19}
$$

where each $U_p(v,\psi,\varsigma)$ is an integral in ρ. The first five expansion functions are tabulated in [10]; for completeness and consistency with the present notation, the first four are repeated here:

$$
\begin{aligned}
U_0(v,\psi,\varsigma) &= \int_0^1 \exp\left[-j\frac{\varsigma\rho^2}{2}\right] J_0(v\rho)\rho d\rho \\
U_1(v,\psi,\varsigma) &= (-j)^m \cos(m\psi) \int_0^1 \exp\left[-j\frac{\varsigma\rho^2}{2}\right] R_n^m(\rho) J_m(v\rho)\rho d\rho \\
U_2(v,\psi,\varsigma) &= \frac{1}{(2)(2!)}\left\{ \int_0^1 \exp\left[-j\frac{\varsigma\rho^2}{2}\right] \left[R_n^m(\rho)\right]^2 \right. \\
&\qquad \left. \times \left[J_0(v\rho) + j^{2m}\cos(2m\psi) J_{2m}(v\rho)\rho d\rho\right] \right\} \\
U_3(v,\psi,\varsigma) &= \frac{1}{(2^2)(2!)}\left\{ \int_0^1 \exp\left[-j\frac{\varsigma\rho^2}{2}\right] \left[R_n^m(\rho)\right]^3 \right. \\
&\qquad \left. \times \left[3(-j)^m \cos(m\psi) J_m(v\rho) + (-j)^{3m}\cos(3m\psi) J_{3m}(v\rho)\right]\rho d\rho \right\}.
\end{aligned} \tag{20}
$$

Nijboer found that for ς and α_{nm} of the order of unity, these four terms provided sufficient accuracy to plot isophote contours. Note that $U_0(u,\psi,\varsigma)$ is the aberration-free focused field predicted by first-order diffraction theory. Inclusion of higher-order terms thus corrects this original field to account for the single aberration under consideration.

For particular primary aberrations, further manipulation of the integrals in (20) using the orthogonality properties of the Zernike circle polynomials were performed to yield closed-form expressions for focused fields in specific receiving planes. The results are somewhat complicated and will not be repeated here. The important result of this approach can be seen from (19) and (20); namely, that by expansion of the aberration function in orthogonal polynomials, and by manipulation of the diffraction integral, the focused field can be expressed as a series of one-dimensional integral terms. Note that if α_{nm} is much larger than unity, the expansion (19) requires a large number of terms to start converging and hence is not suitable. Maréchal addressed this case for large spherical aberration [8] with the use of a mechanical integrator, and some of his isophote contour plots are reproduced in [9].

V. THE FOURIER OPTICS APPROACH

The Fourier optics approach to the focused beam problem differs from the classical approach in two ways. First, it explicitly retains the optical system parameters in the derivation, and second, it is directed toward calculation on digital computing equipment using computationally efficient algorithms. This chapter, which presents the theory behind this approach, is divided into three parts. The first part discusses the analysis of the effects of the focusing lens for greater accuracy than that given in Chapter III. The second and third parts present two approaches for calculating the field in the focal region from the propagation of the field transmitted through the lens to focus according to the Rayleigh-Sommerfeld diffraction integral.

A. Effects of the Lens

The first step in the analysis is to account for the the focusing and aberrating effects of the lens on the transmitted field. As in Chapter III, the thin lens approximation is assumed valid so that, other than the apodization by the lens pupil, the incident and transmitted fields are related by a multiplicative phase relationship. If the thickness function $\Delta(x, y)$ given in (6) is expanded in a Taylor's series, and second-order terms are also retained, a better approximation to the lens thickness than (7) is found to be

$$\Delta(x,y) \cong \Delta_o - \frac{x^2+y^2}{2}\left(\frac{1}{R_1} - \frac{1}{R_2}\right) - \frac{(x^2+y^2)^2}{8}\left(\frac{1}{R_1^3} - \frac{1}{R_2^3}\right). \tag{21}$$

With the definition of the focal length (8), this expression can be substituted into (5) to yield the multiplicative phase transformation relating the incident and transmitted fields for a lens to greater accuracy as

$$\begin{aligned} U(x,y,\Delta_o) \cong\ & U(x,y,0)P(x,y)\exp\left[-j\frac{\pi}{\lambda f}(x^2+y^2)\right] \\ & \times \exp\left[-j\frac{\pi}{4\lambda f}\left(\frac{1}{R_1^2} + \frac{1}{R_1 R_2} + \frac{1}{R_2^2}\right)(x^2+y^2)^2\right]. \end{aligned} \tag{22}$$

The additional phase term gives rise to the primary spherical aberration introduced by the lens [16]. However, further aberrations, including additional spherical aberration, also arise in the propagation of the field to the focal region. These effects will become apparent in the discussion to follow.

What remains in the problem is how efficiently to implement the Rayleigh-Sommerfeld diffraction integral (4) to calculate the field in the focal region. Two approaches, one based upon the two-dimensional convolution integral and the other based upon the Fourier transform integral are presented in the sections that follow. The conditions for applicability for each of these approaches are also discussed.

B. Propagation to the Focal Region: The Convolution Approach

One approach to the calculation of the field in the focal region is to cast the Rayleigh-Sommerfeld formula into the form of a two-dimensional convolution integral. This approach has the advantage that it includes the effects of all aberrations upon the focused field. Its disadvantage is that it is still computationally long, even when implemented using efficient convolution algorithms.

From the Rayleigh-Sommerfeld integral given in (4) and the geometrical definition of terms illustrated in Fig. 1, the vector distance r_{01} from the point (x, y, Δ_o) to the point (x_f, y_f, z_f) can be seen to be given by (11) where, again, the propagation distance z_p is given by $z_p = |z_f - \Delta_o|$. By similar geometric considerations, the obliquity factor $\cos(\mathbf{n}, \mathbf{r}_{01})$ is given by

$$\cos(\mathbf{n}, \mathbf{r}_{01}) = \frac{z_p}{\sqrt{(x_f - x)^2 + (y_f - y)^2 + z_p^2}}. \tag{23}$$

If (11) and (23) are substituted into the Rayleigh-Sommerfeld integral (4) with the change of notation $(x_1, y_1, z_1) = (x, y, \Delta_o)$ and $(x_0, y_0, z_0) = (x_f, y_f, z_f)$ and the definition for the propagation distance z_p given above, the equation for the focused field can be written as

$$U(x_f, y_f, z_f) = \int_{-\infty}^{\infty}\int_{-\infty}^{\infty} U(x, y, \Delta_o) \frac{z_p}{j\lambda} \frac{\exp\left[jk\sqrt{(x_f - x)^2 + (y_f - y)^2 + z_p^2}\right]}{(x_f - x)^2 + (y_f - y)^2 + z_p^2} dxdy. \tag{24}$$

Equation (24) can be more easily recognized as a two-dimensional convolution by defining the function

$$V(x_f, y_f, z_p) \equiv \frac{z_p}{j\lambda} \frac{\exp\left[jk\sqrt{x_f^2 + y_f^2 + z_p^2}\right]}{x_f^2 + y_f^2 + z_p^2}, \tag{25}$$

in which case (24) can be compactly written

$$U(x_f, y_f, z_f) = \int_{-\infty}^{\infty} \int_{-\infty}^{\infty} U(x, y, \Delta_o) V(x_f - x, y_f - y, z_p) dx dy. \tag{26}$$

Equation (26) is the two-dimensional convolution of the transmitted field, expressed in terms of the focal region coordinates x_f and y_f, with the function $V(x_f, y_f, z_p)$ defined in (25). To calculate the field at (x_f, y_f, z_f) from the field transmitted through the lens, it is thus necessary to generate the function $V(x_f, y_f, z_p)$ and convolve it with $U(x_f, y_f, \Delta_o)$. This can be efficiently performed with Fourier transforms using the property that convolution in the signal domain corresponds to multiplication in the frequency domain. If $\mathcal{F}\{.\}$ denotes the two-dimensional Fourier transform operator defined by

$$\mathcal{F}\{g(x, y)\} \equiv \int_{-\infty}^{\infty} \int_{-\infty}^{\infty} g(x, y) \exp\left[-j2\pi(xf_x + yf_y)\right] dx dy, \tag{27}$$

for arbitrary function $g(x, y)$, then the focused field can be expressed as

$$U(x_f, y_f, z_f) = \mathcal{F}^{-1}\{\mathcal{F}\{U(x_f, y_f, \Delta_o)\}\mathcal{F}\{V(x_f, y_f, z_p)\}\}, \tag{28}$$

which says that the focused field at the distance z_p from the back surface of the lens can be calculated by Fourier transforming the field transmitted through the lens, generating the function $V(x_f, y_f, z_p)$ and Fourier transforming it, multiplying the two transforms, and inverse Fourier transforming the result.

As mentioned above, this approach has the distinct advantage that it includes all aberrations in the calculation. This results from the fact that it is an "exact" evaluation of the Rayleigh-Sommerfeld diffraction integral; no approximations were made in the derivation. However, the process of generating a two-dimensional function, performing two two-dimensional Fourier transforms, multiplying the results, and inverse Fourier transforming the product is computationally time-consuming. A further property of this approach when it is discretized for implementation on digital computers, that of no increase in resolution in the calculated focused field, is discussed in the following chapter. This property limits the range of applicability of this approach as a computational technique. Still, it has proven useful for analyzing the effects of the off-axis aberrations – coma, astigmatism, field curvature, and distortion – on large F-number optical systems.

C. Propagation to the Focal Region: The Transform Approach

Another approach to calculating the field in the focal region resulting from the field transmitted through the lens is to approximate the Rayleigh-Sommerfeld diffraction integral so as to manipulate the resulting integral into the form of a two-dimensional Fourier transform. This approach differs from the approach described previously in that rather than using the Fourier transform as a computational tool in evaluating a convolution, the diffraction integral itself is calculated as a Fourier transform. This method has the advantage of computational speed, at the expense of decreased accuracy. The only aberration retained in the derivation is primary spherical aberration. However, for most applications where focusing of a laser beam is employed, spherical aberration is the predominant effect degrading the intensity distribution, and so this approach has proven to be the more useful of the two methods presented here in light of its computational efficiency.

The first two approximations in this approach are the same as that of conventional first-order diffraction theory, namely that in the denominator of the diffraction integral, $r_{01} \cong z_p$, and that the obliquity factor $\cos(\mathrm{n}, \mathrm{r}_{01}) \cong 1$. In the complex exponential term, the distance r_{01} is again expanded in a Taylor's series, and consistent with the approximation for the effects of the lens, terms to second order are retained. Explicitly, the second-order expansion for r_{01} is given by

$$r_{01} \cong z_p + \frac{(x_f - x)^2 + (y_f - y)^2}{2z_p} - \frac{\left[(x_f - x)^2 + (y_f - y)^2\right]^2}{8z_p^3}. \tag{29}$$

Expansion of the third term on the right-hand side of (29) results in several cross-products in x, y, x_f, and y_f. If the region of interest is restricted to a small region about the optical axis where x_f and y_f are small, as is the case in most focusing applications, these cross-products can be neglected. The distance r_{01} can then be further approximated for practical focusing applications by

$$r_{01} \cong z_p + \frac{(x_f - x)^2 + (y_f - y)^2}{2z_p} - \frac{(x^2 + y^2)^2}{8z_p^3}. \tag{30}$$

This dropping of cross-terms in the expansion is equivalent to including only primary spherical aberration in the analysis, and neglecting all other aberrations [9], [10].

Upon substitution of these approximations into the Rayleigh-Sommerfeld diffraction integral, several terms can be brought outside the integral. As in Chapter III, since the functional form of the intensity is the quantity of interest, phase terms and constants can be dropped from the equation for simplicity. The resulting expression for the focused field resulting from the transmitted field is thus

$$U(x_f, y_f, z_f) \sim \frac{1}{z_p} \int_{-\infty}^{\infty} \int_{-\infty}^{\infty} U(x, y, \Delta_o) \exp\left[j \frac{\pi}{\lambda z_p} \left((x^2 + y^2) - \frac{(x^2 + y^2)^2}{4 z_p^2} \right) \right]$$
$$\times \exp\left[-j \frac{2\pi}{\lambda z_p} (x x_f + y y_f) \right] dx dy. \tag{31}$$

Equation (31) can be recognized as being in the form of a Fourier transform integral (27) with the frequency variables given by $f_x = x_f/\lambda z_p$ and $f_y = y_f/\lambda z_p$. Thus, the focused field can be expressed as

$$U(x_f, y_f, z_f) = \mathcal{F}\left\{ U(x, y, \Delta_o) \exp\left[j \frac{\pi}{\lambda z_p} \left((x^2 + y^2) - \frac{(x^2 + y^2)^2}{4 z_p^2} \right) \right] \right\}, \tag{32}$$

with the appropriate substitution for the frequency variables.

Comparison of (32) with (28) clearly suggests that this approach requires considerably less computation time than the convolution approach. Another advantage, which will be shown in the next chapter, is that when the equation is discretized and implemented with discrete Fourier transform techniques, the focused field is calculated at higher resolution than the input transmitted field. The effects of the approximations made in deriving this result, and the omission of off-axis aberrations have not been found to affect the accuracy of the resulting intensity distribution significantly. For these reasons, this approach has become the preferred approach for calculating the focused intensity distribution.

VI. COMPUTATIONAL CONSIDERATIONS

As stated previously, the Fourier optics approach to the laser beam focusing process in the presence of aberrations is directed toward computation on digital computing hardware. Thus, the equations developed in the preceding chapter must be discretized and the implementation carried out so as to be as computationally efficient as possible. Because of the availability and utility of vector array processors, the implementation itself is tailored toward vector processing algorithms. This approach has proven useful by allowing calculations to be carried out on a microcomputer-based image processor, where the resulting intensity distributions could be displayed for visual observation.

The discretization begins by sampling the fields in the given plane of interest. Since no special geometric considerations exist, a uniform rectangular sampling scheme is appropriate. Thus, the following notation for the optical fields will be adopted. For the field incident on the lens, let

$$u_i(m,n) \equiv U(mT, nT, 0); \quad -N/2 \leq m,n \leq N/2 - 1, \tag{33}$$

where T is the sampling interval in both the x and y coordinates, and N^2 is the total number of points in the sampled array. This step assumes that the field is bounded within an $NT \times NT$ area. Similarly, the sampled field transmitted through the lens is denoted

$$u_t(m,n) \equiv U(mT, nT, \Delta_o); \quad -N/2 \leq m,n \leq N/2-1. \tag{34}$$

And the field in the focal region is given by

$$u_f(p,q;z_p) \equiv U(pT_f, qT_f; z_f); \quad -N/2 \leq p,q \leq N/2. \tag{35}$$

Note that the sampling interval T for the incident and transmitted fields is the same, while the sampling interval for the focused field T_f could, in general, be different.

The remainder of this chapter will describe how the equations of Chapter V are implemented in discrete computations. The organization is the same as that of Chapter V. The calculation of the effects of the lens will be treated first, then the calculation of the field in the focal region via the convolution and transform approaches will be presented.

A. Calculation of the Effects of the Lens

By uniform sampling of (22), the field transmitted through the lens can be shown to be given by

$$\begin{aligned} u_t(m,n) =& u_i(m,n) P(mT,nT) \exp\left[-j\frac{\pi T^2}{\lambda f}(m^2+n^2)\right] \\ &\times \exp\left[-j\frac{\pi T^4}{4\lambda f}\left(\frac{1}{R_1^2}+\frac{1}{R_1 R_2}+\frac{1}{R_1^2}\right)(m^2+n^2)^2\right]. \end{aligned} \tag{36}$$

The most time-consuming part of this computation is the calculation of the complex phase terms. To minimize these calculations, define

$$c(m) \equiv \exp\left[-j\frac{\pi T^2}{\lambda f}m^2\right] \tag{37}$$

$$d(m,n) \equiv \exp\left[-j\frac{\pi T^4}{4\lambda f}\left(\frac{1}{R_1^2}+\frac{1}{R_1 R_2}+\frac{1}{R_2^2}\right)(m^2+n^2)^2\right]. \tag{38}$$

Then, (36) can be written

$$u_t(m,n) = u_i(m,n)P(mT,nT)c(m)c(n)d(m,n). \tag{39}$$

Note that the same $c(m)$ array can be used to multiply both the rows and the columns of the incident field array $u_i(m,n)$, and that it need only be computed for positive values of m. This portion of the calculation is vectorizable, and can be carried out by vector-vector multiplication of the n^{th} row of $u_i(m,n)$ by the array $c(m)$, and then scalar-vector multiplication of the n^{th} row by $c(n)$.

Calculation of the array $d(m,n)$ is more time-consuming, but can be minimized by noting that $d(m,n) = d(\pm m, \pm n)$ and that $d(m,n) = d(n,m)$. These properties can be used to reduce calculation of $d(m,n)$ to approximately $N^2/8$ points, out of the total N^2 points in the complex field array. For each row of $u_i(m,n)$, a suitable N-point array must be composed from the appropriate calculated elements of $d(m,n)$, and vector-vector multiplied times the row.

B. Calculation of the Focused Field Using the Convolution Approach

The calculation of the focused field using the convolution approach is simply a discrete approximation to the convolution integral in (26). If the x and y variables are sampled at the interval T, and the integral is approximated by a rectangular-rule summation, (26) becomes

$$U(x_f, y_f, z_f) \cong \sum_{m=-N/2}^{N/2-1} \sum_{n=-N/2}^{N/2-1} U(mT, nT, \Delta_o) V(x_f - mT, y_f - nT, z_p) T^2. \quad (40)$$

Now, if the variables x_f and y_f are sampled at the same interval as x and y, so that $T_f = T$, then the sampled focused field defined in (35) can be written

$$u(p, q; z_p) \cong \sum_{m=-N/2}^{N/2-1} \sum_{n=-N/2}^{N/2-1} u_t(m, n) v(p - m, q - n; z_p), \quad (41)$$

where $v(m, n; z_p)$ is the function $V(x_f, y_f, z_p)$ defined in (25) sampled at the interval T:

$$v(m, n; z_p) \equiv \frac{z_p T^2}{j\lambda} \frac{\exp\left[jk\sqrt{(m^2 + n^2)T^2 + z_p^2}\right]}{(m^2 + n^2)T^2 + z_p^2}. \quad (42)$$

Equation (41) is a two-dimensional discrete convolution of the arrays $u_t(m, n)$ and $v(m, n; z_p)$, and so can be evaluated by a similar frequency-domain method as that discussed in Chapter V, Section B. The only difference is that discrete

Fourier transforms are used rather than continuous Fourier transforms. If $\mathcal{F}_D\{.\}$ denotes the discrete two-dimensional Fourier transform defined by

$$\mathcal{F}_D\{g(m,n)\} \equiv \sum_{m=-N/2}^{N/2-1} \sum_{n=-N/2}^{N/2-1} g(m,n) \exp[-j2\pi(mp+nq)/N], \tag{43}$$

then $u_f(p,q;z_p)$ can be evaluated by

$$u_f(p,q;z_p) = \mathcal{F}_D^{-1}\big\{\mathcal{F}_D\{u_t(m,n)\}\mathcal{F}_D\{v(m,n;z_p)\}\big\}. \tag{44}$$

The two-dimensional discrete Fourier transforms in (44) can be carried out using the fast Fourier transform (FFT) algorithm. The major computational burden in this approach is the calculation of the array $v(m,n;z_p)$. This can be minimized by noting that it has the same circularly symmetric properties as the $d(m,n)$ array discussed in the previous section, and so only $N^2/8$ points need actually be computed out of the N^2 points in the full array.

As a final consideration, the arrays $u_t(m,n)$ and $v(m,n;z_p)$ must be zero-padded to prevent the "wraparound" effect associated with the circular convolution performed by discrete Fourier transforms [23]. That is, both $N \times N$ arrays must be extended to $2N \times 2N$ arrays by filling in the extra points with zero values. The discrete Fourier transforms must then be performed with $2N$-point FFT algorithms applied to the zero-padded arrays. This results in a relatively high memory storage requirement on the computer hardware, and the value of N must be chosen so as not to exceed the storage capabilities of the hardware.

As mentioned in Chapter V, this technique has the property that the sampling interval of the focused field is equal to the sampling interval of the input transmitted field. In general, this is undesirable since the extent of a focused beam is usually much smaller than that of the beam incident on the lens, and thus to examine its intensity distribution, the sampling interval must be correspondingly small. However, cases do exist for large F-number systems where this effect is not overly detrimental, and this computational technique is quite useful for such applications, for it does have the advantage that it includes all aberrations in the analysis. The generation of the function $v(m, n; z_p)$ is computationally long, as are the three discrete Fourier transforms required for its implementation. The primary application of this technique is the examination of off-axis aberrations in transverse-plane intensity distributions for large F-number focusing systems.

C. Calculation of the Focused Field Using the Transform Approach

The calculation of the focused field using the transform approach involves proper discretization of (31). As in the preceding section, the variables x and y are sampled at interval T and the integral approximated by a rectangular-rule finite summation. With the substitution of the sampled transmitted field given in (34), the functional form of the focused field can be approximated by

$$U(x_f, y_j, z_f) \sim \frac{1}{z_p} \sum_{m=-N/2}^{N/2-1} \sum_{n=-N/2}^{N/2-1} u_t(m,n) \exp\left[j\frac{\pi T^2}{\lambda z_p}(m^2+n^2)\right] \times \exp\left[-j\frac{\pi T^4}{4\lambda z_p^3}(m^2+n^2)^2\right] \times \exp\left[-j\frac{2\pi T}{\lambda z_p}(mx_f+ny_f)\right] \tag{45}$$

If the field in the focal region is now sampled as given in (35) with sampling interval T_f chosen to be

$$T_f = \frac{\lambda z_p}{NT}, \tag{46}$$

then the sampled focused field can be written

$$u_f(p,q;z_p) \sim \frac{1}{z_p} \sum_{m=-N/2}^{N/2-1} \sum_{n=-N/2}^{N/2-1} u_t(m,n) \exp\left[j\frac{\pi T^2}{\lambda z_p}(m^2+n^2)\right] \times \exp\left[-j\frac{\pi T^4}{4\lambda z_p^3}(m^2+n^2)^2\right] \times \exp[-j2\pi(mp+nq)/N]. \tag{47}$$

Equation (47) can be recognized as being a two-dimensional discrete Fourier transform, and thus the focused field can be calculated from the transmitted field array using the FFT algorithm. Multiplication of the transmitted field array by the first and second complex phase terms in (47) can be performed using the same technique as that described in Section A of this chapter. This computational technique is considerably faster and requires less memory storage than the convolution approach.

Because of the computational speed of this approach, it has proven useful for examining the focusing process by calculating the intensity distribution in the meridional plane, a technique originally used by Nijboer and Zernike and later adopted by Maréchal, as well as more recent authors. This involves calculating a "slice" of the field in say, the (y_f, z_f)-plane, with $x_f = 0$, which illustrates the behavior of the radiation as the field propagates toward focus. Substituting $p = 0$ into (47) shows that for each distance z_p, the following calculation must be performed:

$$
\begin{aligned}
u_f(0, q; z_p) \sim \frac{1}{z_p} \sum_{n=-N/2}^{N/2-1} \Bigg\{ \sum_{m=-N/2}^{N/2-1} & u_t(m, n) \exp\left[j \frac{\pi T^2}{\lambda z_p} (m^2 + n^2) \right] \\
& \times \exp\left[-j \frac{\pi T^4}{4 \lambda z_p} (m^2 + n^2)^2 \right] \Bigg\} \qquad (48) \\
& \times \exp(-j 2\pi n q / N).
\end{aligned}
$$

The inner summation over m contained within curly brackets in the equation above results in an N-point sequence in the index variable n, and the calculation involving n can be recognized as a one-dimensional N-point discrete Fourier transform. Provided that the inner summation can be calculated efficiently, the computational requirements of the one-dimensional discrete Fourier transform is almost negligible.

The major part of this computational burden lies in the calculation of the complex phase terms. The first term, involving only m^2+n^2, can be calculated by defining an N-point array similar to the array $c(m)$ defined in (37), calculating it only for positive values of m, and performing the vector-vector and scalar-vector multiplication of the n^{th} row of the two-dimensional array as described previously.

Calculation of the second phase term involving $(m^2+n^2)^2$ is more difficult, and can be prohibitively long if the calculation is to be performed for many values of the propagation distance z_p. This problem can be overcome in the following way. In general, the intensity distribution is only of interest in a small region near focus where $z_p \cong f$. If this approximation can be assumed to be valid over the range of z_p used in the calculation of the meridional plane field distribution, then the transmitted field $u_t(m,n)$ can be replaced by an altered transmitted field array $u_t'(m,n)$ defined by

$$u_t'(m,n) \equiv u_t(m,n) \exp\left[-j\frac{\pi T^4}{4\lambda f^3}(m^2+n^2)^2\right]. \tag{49}$$

In fact, this calculation can be incorporated into the calculation of the transmitted field (39) by defining

$$d'(m,n) \equiv \exp\left[-j\frac{\pi T^4}{4\lambda f}\left(\frac{1}{R_1^2}+\frac{1}{R_1R_2}+\frac{1}{R_2^2}+\frac{1}{f^2}\right)(m^2+n^2)^2\right], \tag{50}$$

in which case the altered transmitted field can be written

$$u_t'(m,n) = u_i(m,n)P(mT,nT)c(m)c(n)d'(m,n), \tag{51}$$

with $c(m)$ as given in (37). Note that this step involves the assumption that the spherical aberration affecting the focused field near the paraxial focus arises from the inclusion of the additional phase term given in (50), and that it results from both the spherical surfaces of the focusing lens and from the propagation properties of the electromagnetic radiation.

With this approximation for computational speed, (48) can be written

$$\begin{aligned} u_f(0,q;z_p) \sim \frac{1}{z_p} \sum_{n=-N/2}^{N/2-1} \sum_{m=-N/2}^{N/2-1} u_t'(m,n) \exp\left[j\frac{\pi T^2}{\lambda z_p}(m^2+n^2)\right] \\ \times \exp(-j2\pi nq/N). \end{aligned} \tag{52}$$

This equation expresses the procedure for computing the focused field in the meridional plane. The altered transmitted field array $u_t'(m,n)$ is multiplied row-wise and column-wise by a quadratic complex phase term, summed over the index variable m, and the resulting N-point sequence transformed with a one-dimensional discrete Fourier transform. This procedure is repeated for incremented values of the propagation distance z_p to construct an "image" of the field distribution profile in the (y_f, z_f)-plane.

As a final remark regarding this calculation, note the change in sampling interval implied by (46) that exists between the input transmitted field array and the output focused array. This change in sampling interval is usually desirable and can be quite significant. For example, with a wavelength $\lambda = 633$ nm, and using $N = 1024$-point discrete Fourier transforms, the output sampling interval in the focal region of a 13 mm focal length lens is approximately $T_f = 0.25$ μm for an input sampling interval of $T = 32$ μm, a factor of 128 increase in resolution. Also, since T_f is dependent upon the propagation distance z_p, and the image display pixels are uniformly spaced, a meridional plane calculation carried out using this technique will result in a distorted image display. Usually, however, the range of z_p is limited so that the distortion is not significant.

VII. CALCULATED RESULTS

Calculations of transverse and meridional plane intensity distributions have been carried out for several incident laser beam profiles using the equations of Chapter V implemented as described in Chapter VI. These calculations were carried out on a microprocessor-based digital image processor equipped with vector array processing hardware. The digital image processor proved to be a useful device for this purpose because of its large memory storage capabilities and its ability to display calculated results in an easily understandable format. Other image processing techniques such as contrast stretching and pseudocolor were also available to enhance the calculated intensity data for visual interpretation.

To illustrate the utility of the convolution approach to laser focusing, transverse plane intensity distributions in the paraxial focal plane were calculated for a circular beam profile with uniform amplitude across its area. The beam was assumed to have a diameter of 3.75 mm with 633 nm wavelength radiation and incident on a 400 mm focal length plano-convex lens with front radius of curvature $R_1 = 207$ mm. To simulate the effect of small angle misalignment in the focusing system, the incident beam profiles were generated with linear phase shifts in the vertical direction.

Fig. 3 shows the calculated intensity pattern in the paraxial focal plane for an incident beam angle of 0.000 degrees (perfect alignment). While its appearance is similar to that of the familiar Airy disk predicted by first-order diffraction

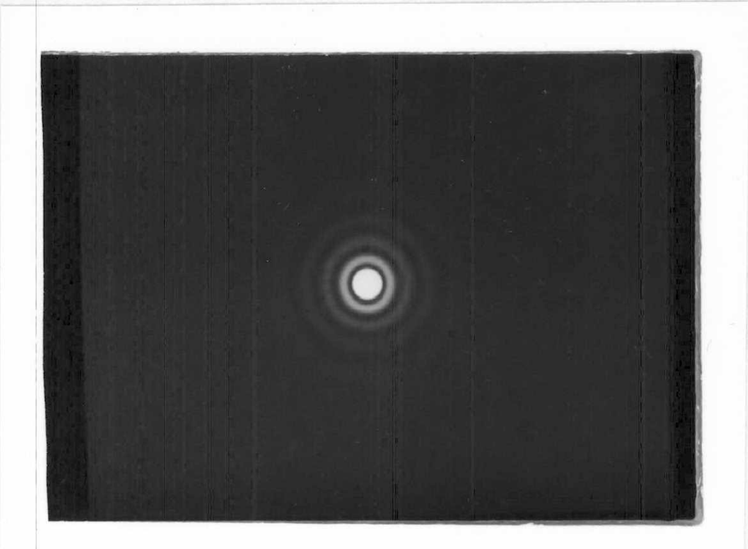

Fig. 3. Calculated focal plane intensity for uniform circular beam incident on lens at 0.000 degrees.

theory, careful examinination will reveal slight discrepancies introduced by the aberrations. The focused intensity distribution for an incident beam angle of 0.069 degrees is shown in Fig. 4. A small amount of asymmetry in the pattern is the effect of coma. Coma flare is quite evident in Fig. 5 which is the focused intensity pattern for an incident angle of 0.138 degrees. In addition, a four-point pattern evident in the first diffraction ring indicates the effect of astigmatism. Both coma and astigmatism are quite evident in the focused field pattern for an incident beam angle of 0.207 degrees shown in Fig. 6. This series of pictures supports the claim made earlier that the convolution approach to calculation of the focused field is primarily of use for examining the off-axis aberrations in large F-number optical systems.

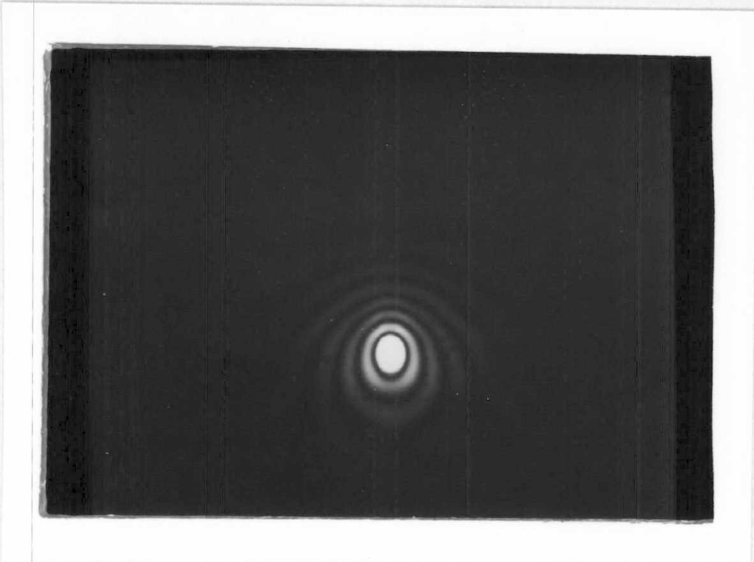

Fig. 4. Calculated focal plane intensity for uniform circular beam incident on lens at 0.069 degrees.

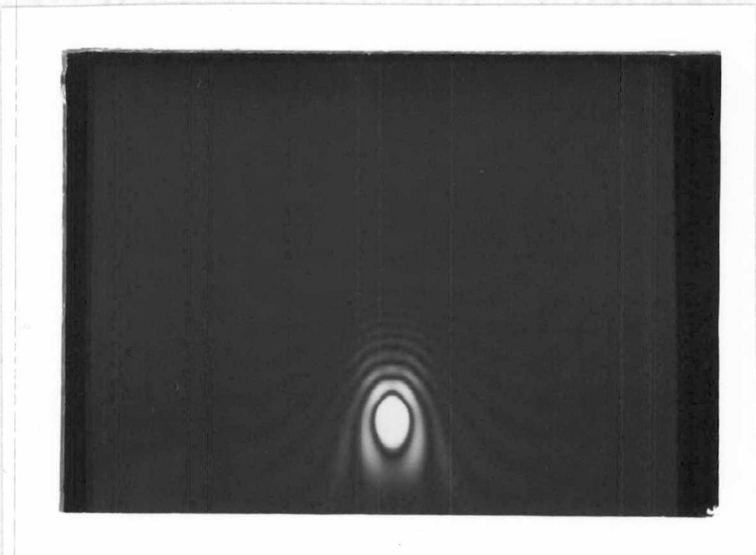

Fig. 5. Calculated focal plane intensity for uniform circular beam incident on lens at 0.138 degrees.

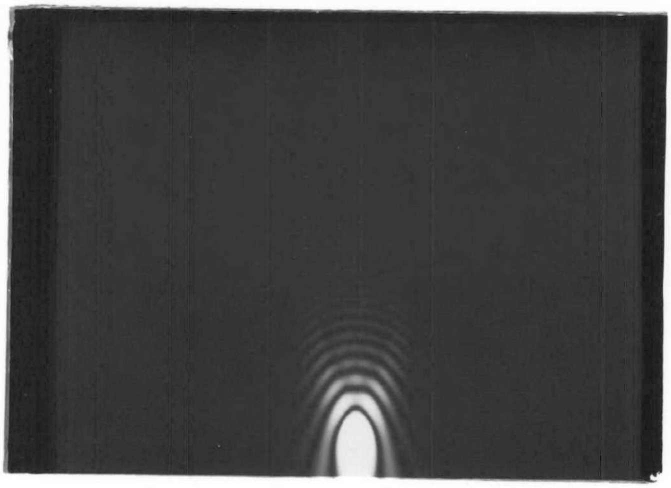

Fig. 6. Calculated focal plane intensity for uniform circular beam incident on lens at 0.207 degrees.

Of perhaps more utility in most laser focusing applications is the use of the transform approach to calculate the meridional plane intensity distribution. In this way, the focusing process of the propagating beam is quite clearly illustrated and understood. This technique has been used for numerous incident beam profiles and some of the results are presented here. The optical system studied was intended to simulate a carbon-dioxide welding laser system with its parameters scaled from the 10.6 μm wavelength CO_2 radiation to 633 nm wavelength HeNe radiation. This system was also studied experimentally as discussed in chapters to follow. The lens for this study was a 13 mm focal length, 6 mm diameter plano-convex lens with front surface radius of curvature $R_1 = 6.8$ mm. The focal region for this system extends from 12.0 to 13.1 mm behind the lens and for a distance of 50 μm above and below the optical axis.

In Fig. 7 the calculated intensity profile resulting from a uniform amplitude circular beam 6 mm in diameter is shown. The light is propagating from left to right in this and all other images shown here. Also, the contrast of some of these images has been enhanced in order to show more clearly some of the details of the diffraction patterns. This image can be compared with the isophote contour plot in Fig. 1 (page 6). Although the field of view and optical system parameters are different for the two figures, similarity exists in the general form of the intensity distributions. This trend is consistent for other plots generated by Maréchal [8] and reproduced in [9]. Note that the spherical aberration causes the region of high intensity to occur in front of paraxial focus, located on the right side of the figure, and that the intensity falls to a low level after focus. The on-axis intensity plot, normalized to unity at the peak intensity location, is shown in Fig. 8.

The meridional plane intensity distribution resulting from a pair of 350 μm diameter pinholes separated by 2 mm and illuminated at a distance of 100 mm in front of the lens is shown in Fig. 9. Again, the effects of spherical aberration are evident: note that the region of high intensity where the beams cross is located in front of paraxial focus, and that the interference fringes are converging as the beams cross. The normalized on-axis intensity plot is shown in Fig. 10.

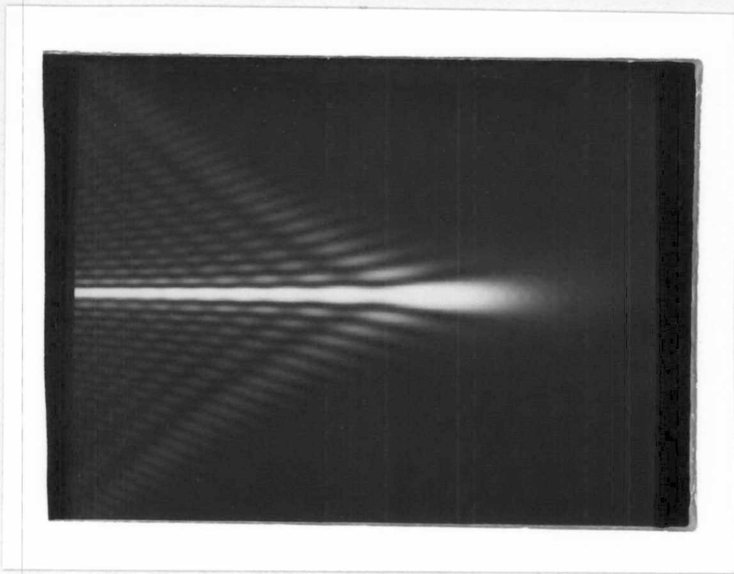

Fig. 7. Calculated meridional plane intensity for uniform circular beam.

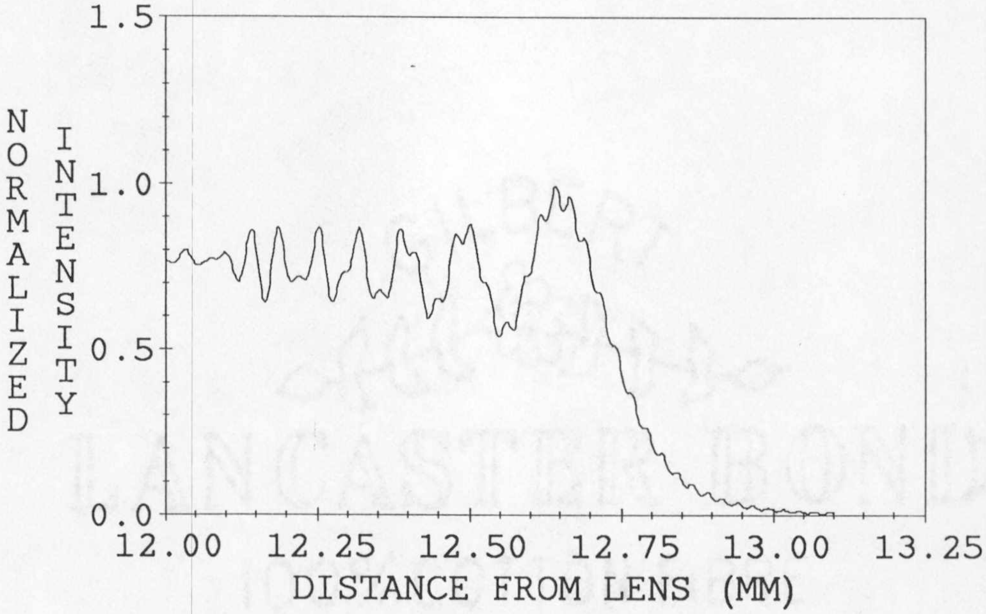

Fig. 8. Normalized on-axis intensity for uniform circular beam.

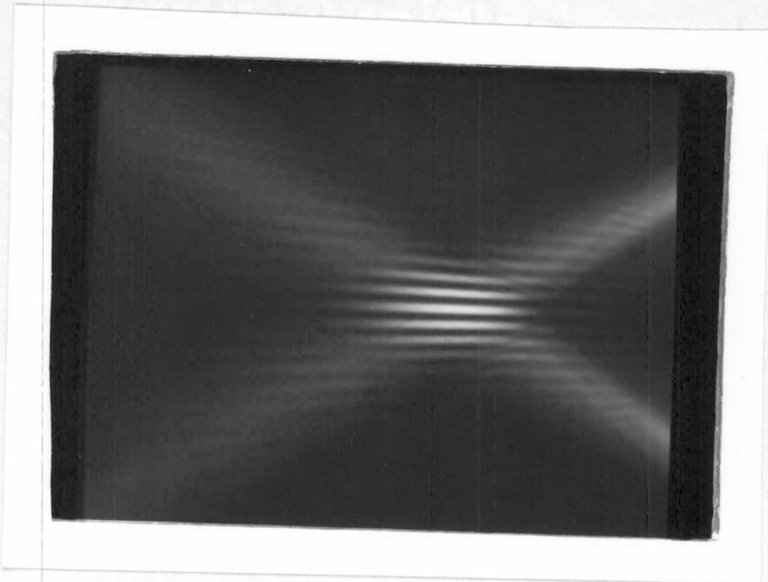

Fig. 9. Calculated meridional plane intensity for two-pinhole beam.

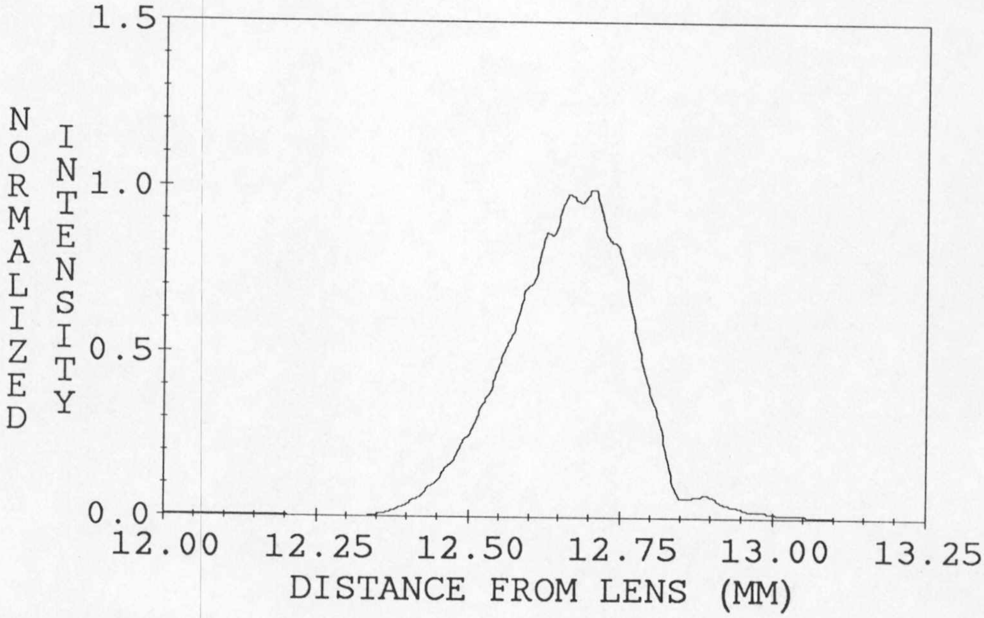

Fig. 10. Normalized on-axis intensity for two-pinhole beam.

An annular beam with 6 mm outside diameter and 2.8 mm inside diameter was used to calculate the intensity distribution shown in Fig. 11. Its on-axis intensity is shown in Fig. 12.

Finally, Fig. 13 shows the meridional plane intensity pattern for a focused 2.5 mm diameter Gaussian beam. Note that the conventional first-order diffraction theory principle that Gaussian beams focus to Gaussian beams is incorrect when spherical aberration is taken into account. The normalized on-axis intensity graph for this case is shown in Fig. 14.

The images shown here illustrate the utility of the transform approach in calculating the intensity distribution of a focused beam in the presence of primary spherical aberration. This technique is most applicable to systems like the one studied here, namely, relatively small F-number focusing systems where spherical aberration is the dominant aberration affecting the focused field. The calculation time for each 512×512 pixel image on the digital image processor described previously was approximately 2 hours and 45 minutes, and required 4 Megabytes of memory.

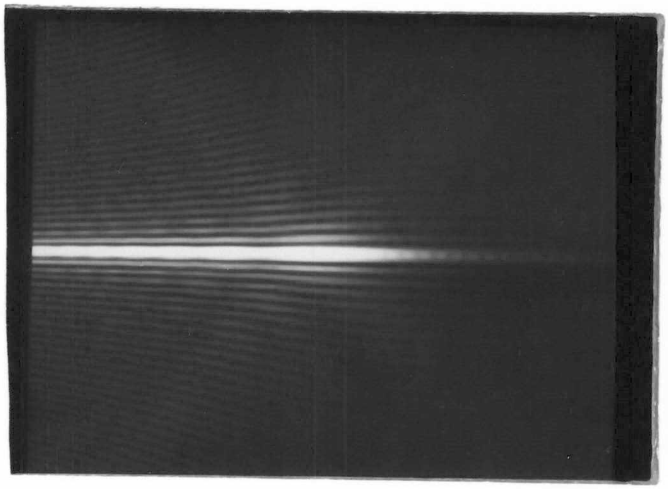

Fig. 11. Calculated meridional plane intensity for annular beam.

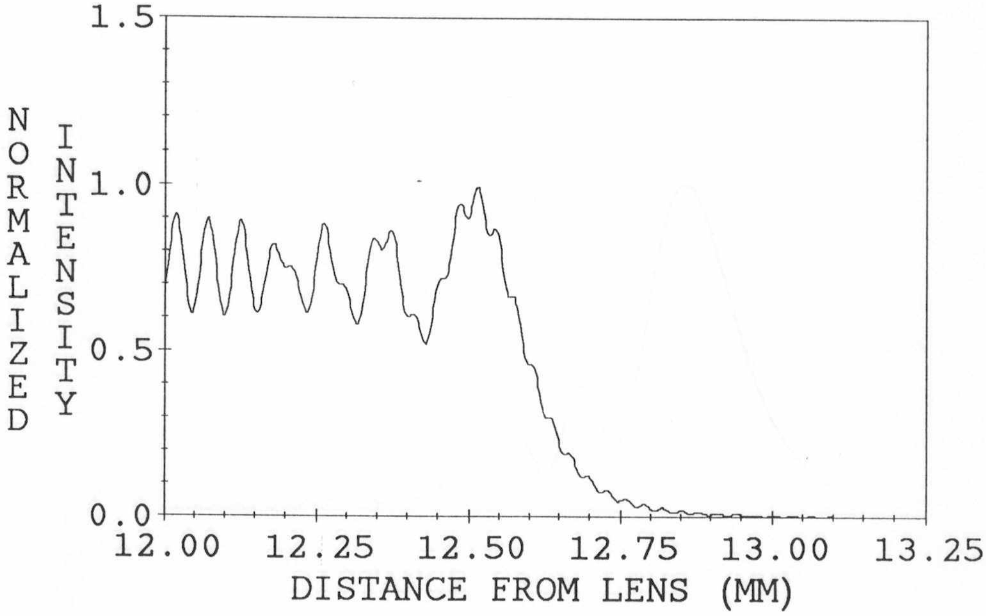

Fig. 12. Normalized on-axis intensity for annular beam.

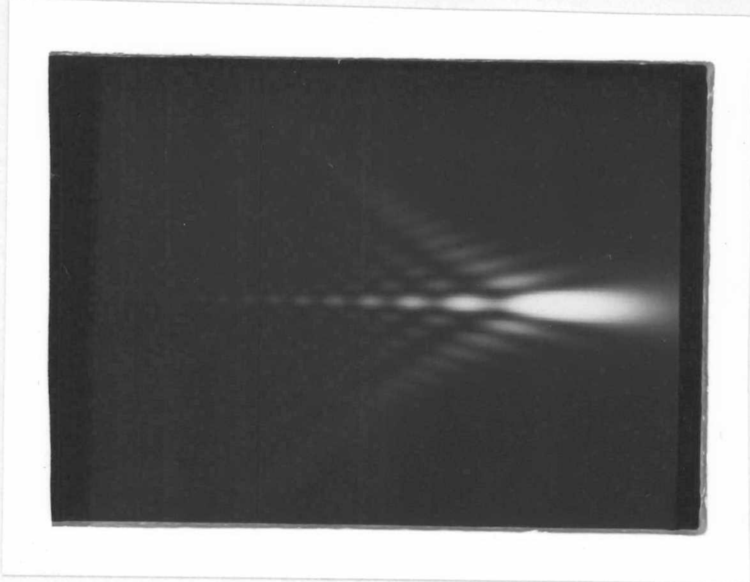

Fig. 13. Calculated meridional plane intensity for Gaussian beam.

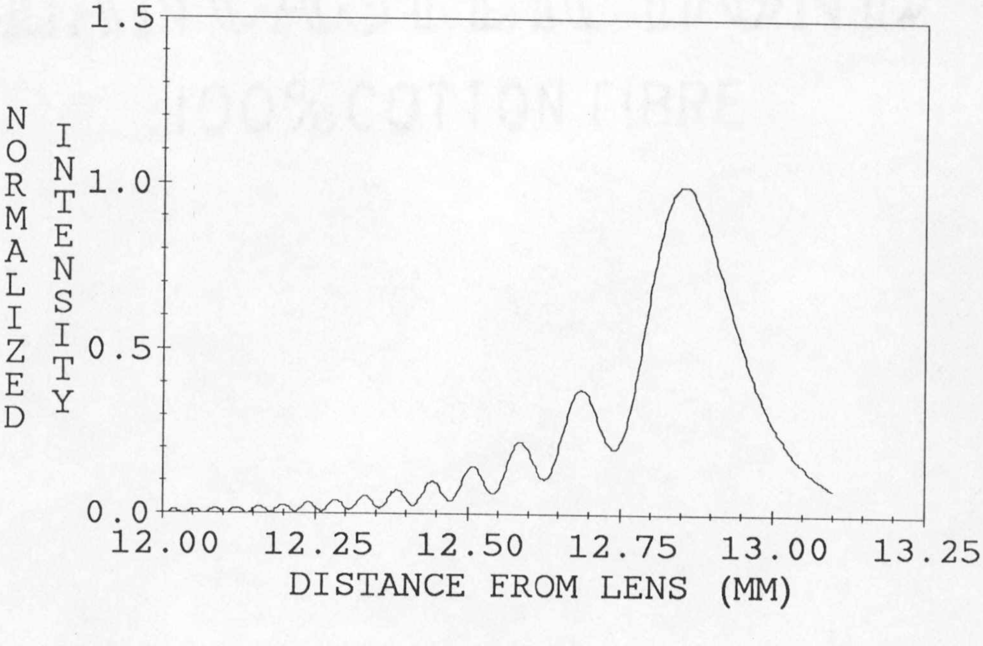

Fig. 14. Normalized on-axis intensity for Gaussian beam.

VIII. LIMITATIONS TO THE APPROACH

At this point, some discussion of the limitations and shortcomings of the Fourier optics approach to the focusing problem is in order. This effort has concentrated on including the effects of the primary aberrations, with emphasis on spherical aberration, into the scalar diffraction theory of focusing a coherent beam. As such, it is by no means a panacea for all optical processing and propagation applications, but is limited in its scope by the assumptions inherent in it. This chapter discusses some of the more important limitations and points out areas for further work.

One limitation to the approach as presented here is that polarization effects have not been considered. This limitation was introduced in Chapter III when the assumption was made that only one component of the electric or magnetic field suffices to characterize the radiation. In general, of course, three components of both the electric and magnetic fields are required to describe a propagating electromagnetic disturbance, and such vector diffraction analysis is beyond the scope of this work.

For many applications, however, the propagating optical disturbance is a transverse wave having only two nonzero components for the electric and magnetic fields, which in turn are strongly coupled. In these cases, the approach taken here may be applicable provided the two components can be considered separately. The lens effects and propagation of each of the field components can be calculated using the approach given here and the focused intensity calculated by the relation

$$I(x_f, y_f, z_f) = |U_x(x_f, y_f, z_f)|^2 + |U_y(x_f, y_f, z_f)|^2, \tag{53}$$

where $U_x(x_f, y_f, z_f)$ denotes the x-component and $U_y(x_f, y_f, z_f)$ denotes the y-component of the electric or magnetic field. This would require twice the computation and twice the memory storage requirements of the single component analysis, however, and may still not be applicable when the components are not behaving independently.

Another limitation is that propagation through inhomogeneous media has not been addressed. This would be advantageous in areas such as laser welding and laser-sustained plasmas, where the media near focus can exhibit variations in its refractive index. However, the problem becomes a complicated three-dimensional one involving the satisfaction of certain boundary conditions that requires computationally intensive iterative numerical schemes to solve in general. To date, this problem has not been addressed.

Finally, mention should be made of the thin lens approximation. This part of the approach is a holdover from first-order scalar diffraction theory, and is clearly an area where improvements to the theory could be made. The thin lens assumption has been found to be valid in many instances, even those for which the thickness of the lens is not negligible. However, for multi-element lens systems or very thick lenses it may not hold. It is unusual that geometric ray-tracing can handle these cases while diffraction theory, normally considered the more exact approach, has difficulty.

Considerable effort was made to overcome this limitation. A scheme that on the face of it, appeared to hold promise, was a hybrid approach whereby the field incident on the front plane of the lens is converted to an array of rays, each of which has given amplitude and phase, and each ray traced through the lens to its proper location in the rear plane of the lens. The phase of each ray in the rear plane could then be determined by calculation of the total optical path length the ray traversed and the field in the rear plane calculated from the amplitude and phase information contained in the ray array.

This approach met with several obstacles. First, determining the direction of a given ray is a difficult task, since it depends on the amplitude and phase distribution in the entire field. Thus, conversion of the incident field to an array of rays is not as straightforward as it may appear. Second, even for cases such as collimated beams where the directions of all the rays are known, the transmitted field calculated in this manner will not be sampled in a uniform rectangular grid. The computational load associated with interpolation of the field to uniform sampling locations becomes prohibitive. Finally, a fundamental drawback with this approach is that it will result in a greater amount of spherical aberration than that predicted by the thin lens approximation. As pointed out by Geary and Petersen [16], the amount of spherical aberration predicted by the thin lens approximation is itself greater than that predicted by geometrical optics. Thus, this technique would result in a grossly overestimated amount of spherical aberration introduced by the lens.

For these reasons, the approach employing the thin lens approximation was retained. Experimental results presented in Chapter X indicate that this approach is still a useful and valid approximation. However, it is limited to simple lens systems, and so is not particularly applicable to extremely thick lenses or multi-element systems.

One curious consequence of the thin lens approximation that can be seen from (22) is that for a given focal length and index of refraction, the amount of spherical aberration introduced by the lens is minimized when $R_1 = -R_2$. That is, according to this approach, spherical aberration is minimal in a biconvex lens with equal front and back radii of curvature. Because this conclusion is in disagreement with geometric ray tracing analyses, even for thin lenses, the approach taken here can be called into question. Still, which approach is "right," in the sense of how accurately it models the behavior of light, cannot be so simply determined, and so remains an area for further research.

IX. EXPERIMENTAL ANALYSIS

An extremely important aspect of this research effort is the experimental analysis conducted to verify the theoretical approach and to develop a usable technique for examining the focusing process. Early work in the experimental investigation of the diffraction theory of aberrations was carried out by Nienhuis [6] who obtained transverse plane intensity distributions near focus in the presence of primary spherical aberration, coma and astigmatism. His photographs are reproduced in [10], and duplication of his results would be of little benefit. Because of the utility of meridional plane intensity distributions in showing the focusing process as the beam propagates toward focus, the experimental analysis conducted in this study concentrated on experimentally acquiring data like the calculated images presented in Chapter VII. The difficulty with acquiring such data is that the meridional plane intensity cannot be seen or imaged by conventional optical imaging instruments.

To acquire meridional plane data, it was necessary to construct the image from a succession of tranverse plane intensity data passing through the optical axis. The technique that was developed was to acquire two-dimensional digital images of the intensity patterns in transverse planes, and to extract the central column from each image. These columns were then successively positioned adjacent to one another to form the meridional plane intensity distribution.

The apparatus for doing this is shown schematically in Fig. 15. The beam from a small helium-neon laser (A) is first passed through a spatial filter and beam expander (B), and strikes a mask (C) that produces the desired incident beam profile. A 13 mm focal length, 6 mm diameter plano-convex lens (D) focuses the incident beam. The imaging lens (E), mounted on a stepper-motor driven translation stage (F), then images the field in the focal zone onto the two-dimensional detector array of a video camera (G).

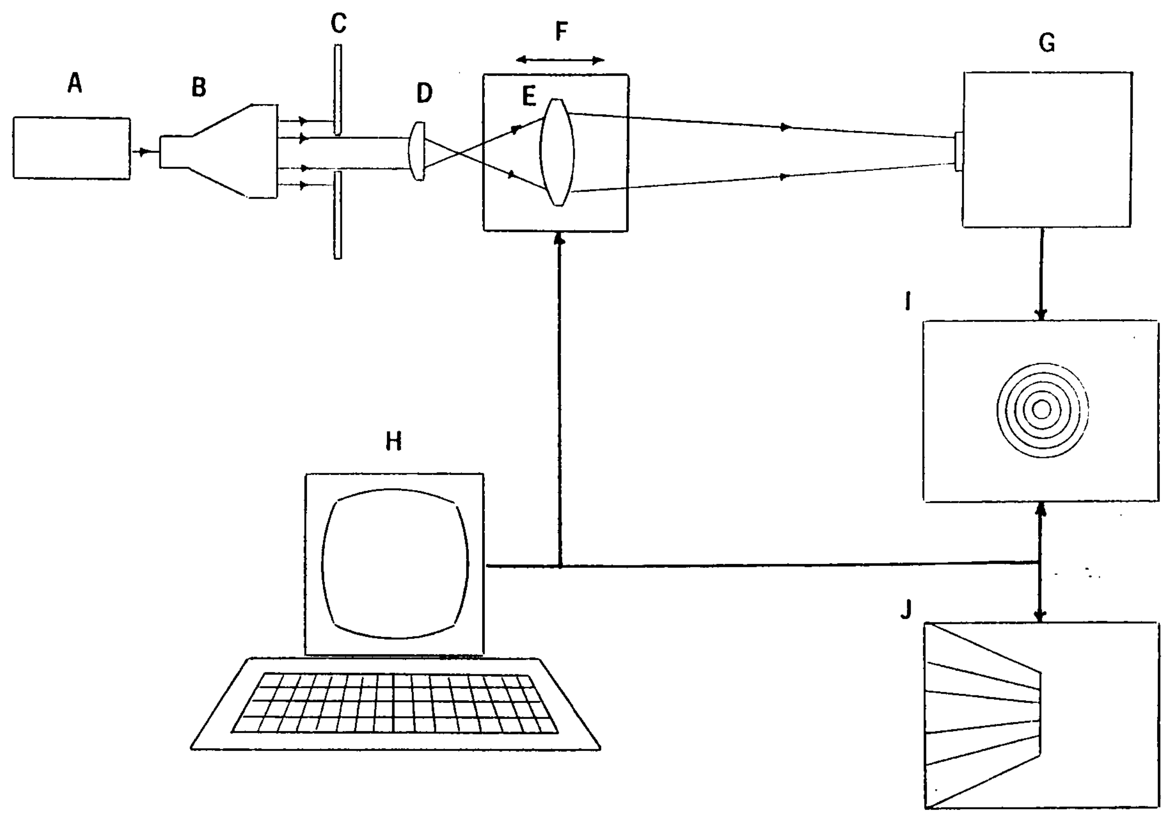

Fig. 15. Apparatus for acquiring meridional plane intensity data.

Because this arrangement is a coherent imaging system, the intensity on the camera detector at the distance d_i from the imaging lens is a magnified reproduction of the intensity in a plane in the focal region at a distance d_o in front of the lens, where the distances d_i and d_o satisfy

$$\frac{1}{d_i} + \frac{1}{d_o} = \frac{1}{f}, \tag{54}$$

and where f is the focal length of the imaging lens. In this arrangement, $d_i \gg d_o$, and the magnification of the system, given by $M = d_i/d_o$, is large enough so that the field within the focal region can be detected at sufficient resolution by the camera. Also, if the distance d_i is changed by moving the imaging lens a small amount Δd_i, then from (54), the distance d_o can be seen to change only by the negligible amount $\Delta d_o = -\Delta d_i/M^2$, and thus remains approximately the same. In this way, different planes in the focal region are imaged onto the camera detector by moving the translation stage a known amount. In the actual setup, the imaging lens was a 25 mm focal length achromatic lens, and $d_i \cong 2.5$ m, so that the magnification M was approximately 100.

The transverse plane intensity data are digitized into 512×512 pixel images by a digital image processor (H) that, in addition, also controls the translation stage (F). The central column from the transverse plane image (I) is then determined and written into the meridional plane image (J). The translation stage is then moved a known amount, in this instance 2.1 μm, and the process is repeated.

Determination of the central column for the transverse plane intensity images was performed in various ways. For radially symmetric beam profiles, a center-of-mass type calculation carried out over the pixel array of the image could be used to find the center of the intensity pattern. This method was susceptible to systematic errors introduced by background bias or slight asymmetry in the focused beam, however. A simpler but more effective technique was to select the location of the maximum pixel value in the image as the center of the beam. For asymmetric beam profiles, very little could be done except to align the beam on a chosen column prior to data acquisition, and to extract the intensity data from that column during the entire course of the data collection procedure.

Data acquisition in this manner was of course sensitive to the alignment of the optical components, vibration, and atmospheric turbulence. Care was thus taken to align and secure the optical components, and a vibration-isolated table helped to reduce mechanical vibrations. Some of the effects of atmospheric turbulence were removed simply by turning off the laboratory ventilation system during data acquisition. As a final step in minimizing these effects, it was sometimes possible to average several meridional plane intensity images, thus reducing the random fluctuations that occurred from image to image.

Two questions that arise about this technique concern the use of an imaging lens to study the aberrations introduced by the focusing lens. First, loss of information could occur from the apodization of the beam by the finite size of the lens. A geometric analysis of the focusing and imaging lens system showed that this effect was negligible, however. Second, aberrations could be introduced by the imaging system itself. These aberrations would result in distortion and misfocusing of the imaged intensity pattern. To be sure, these effects were present, however, the lens was of reasonably high-quality, and the aberrations were not so severe as to result in a grossly erroneous image of the intensity in the focal region. In summary, errors exist in the images obtained by this technique, but they are not believed to alter appreciably the significant features of the intensity distributions.

X. EXPERIMENTAL RESULTS

The experimental apparatus and data acquisition technique described in the preceding chapter were used to obtain several meridional plane intensity distributions. In this chapter, three of these images are presented whose optical system parameters correspond to those of the calculated images shown in Figs. 7, 9 and 11 of Chapter VII (pages 46, 47 and 49, respectively). For each image, the field of view is from $z_p = 12.0$ to 13.1 mm behind the 13 mm focal length focusing lens and extends approximately 50 μm above and below the optical axis. As in Chapter VII, some of these images have been enhanced with digital image processing techniques to increase their visibility and contrast.

Fig. 16 shows the experimental meridional plane intensity for a 6 mm diameter uniform circular beam incident on the lens. Comparison of this image with the calculated image in Fig. 7 (page 46) repeated here in Fig. 17 for the same incident beam profile shows a high degree of agreement in the functional form of the focused intensity. Some discrepancy exists, however, in the overall extent of the distribution and in the angle of the caustic. While this may result from limitations of the theory, it may also be caused by the tolerance limits in the manufacturer's specifications for the lens, which are stated as being $\pm$ 5 per cent of their nominal values. Fig. 17 was calculated assuming a perfectly spherical surface lens with a focal length of exactly 13 mm. The agreement between the theory and experiment is quite good in spite of this slight difference.

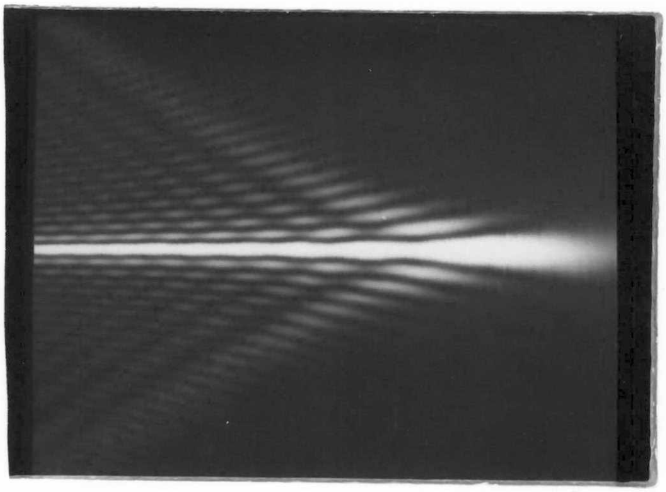

Fig. 16. Experimental meridional plane intensity for uniform circular beam.

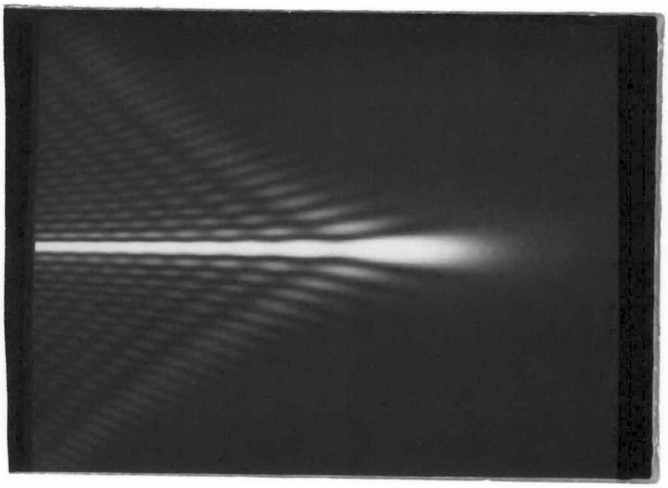

Fig. 17. Calculated meridional plane intensity corresponding to Fig. 16.

A two-pinhole mask with 350 μm diameter pinholes separated on centers by 2 mm and placed 100 mm in front of the focusing lens was used to obtain the meridional plane intensity pattern shown in Fig. 18. Comparison with the calculated image in Fig. 9 (page 47) reproduced in Fig. 19 again shows strong agreement between theory and experiment. Note some of the effects of vibration or air turbulence during the data acquisition procedure that are evident in the center of the image.

Finally, an annular beam with 6 mm outside diameter and 2.8 mm inside diameter produced the focused meridional plane intensity shown in Fig. 20. This may be compared with Fig. 11 (page 49), which displays the calculated intensity distribution for this same case, and is reproduced for convenience in Fig. 21.

These images clearly demonstrate the validity of the Fourier optics approach to aberrations in focused laser beams. The strong agreement, both qualitatively in terms of the similarity of the functional forms of the intensity distributions, and quantitatively in terms of their physical extents, indicates that for practical focusing systems, the calculation techniques presented here can successfully predict the focused field inclusive of the effects of spherical aberration. Further, these images provide experimental data depicting the focusing process that has been lacking since the earliest work in the diffraction theory of aberrations.

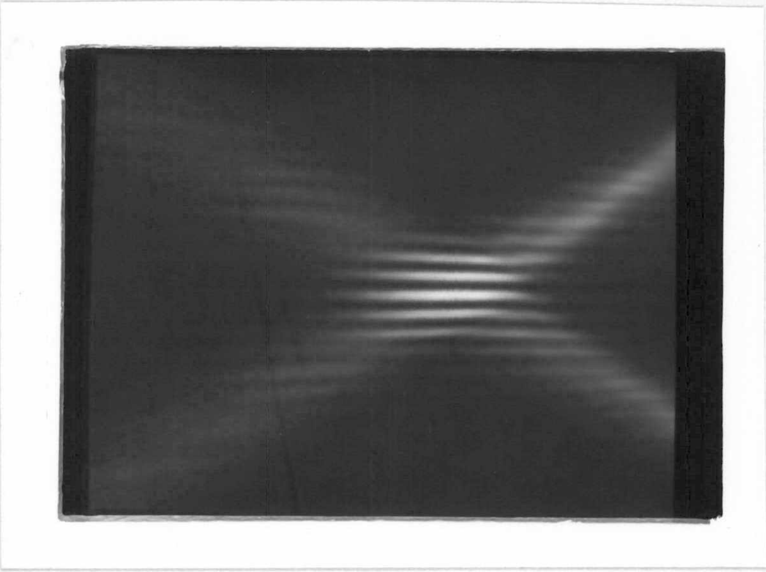

Fig. 18. Experimental meridional plane intensity for two-pinhole beam.

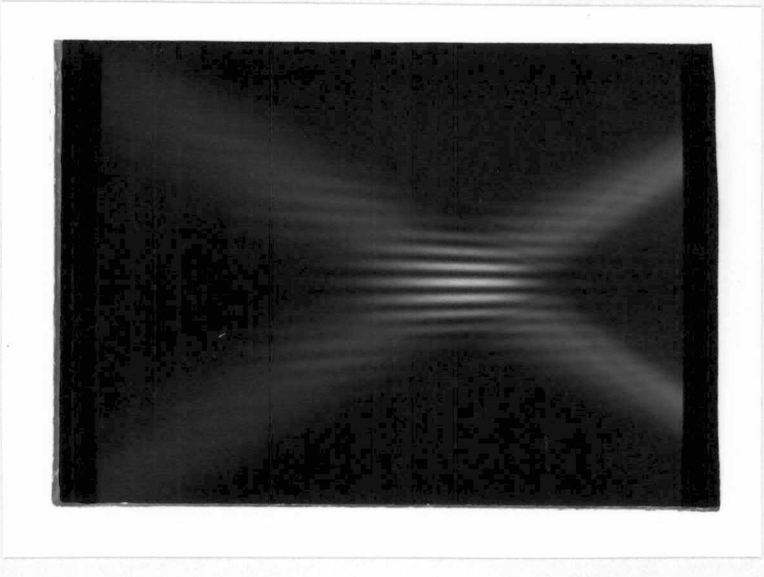

Fig. 19. Calculated meridional plane intensity corresponding to Fig. 18.

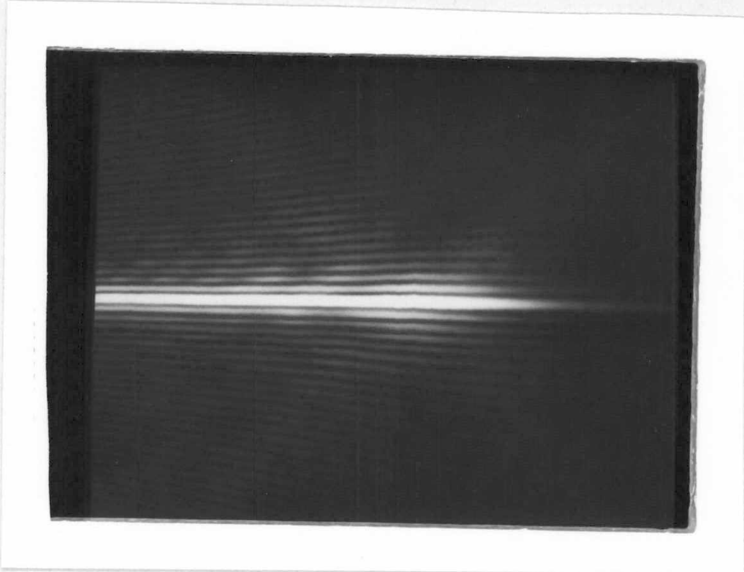

Fig. 20. Experimental meridional plane intensity for annular beam.

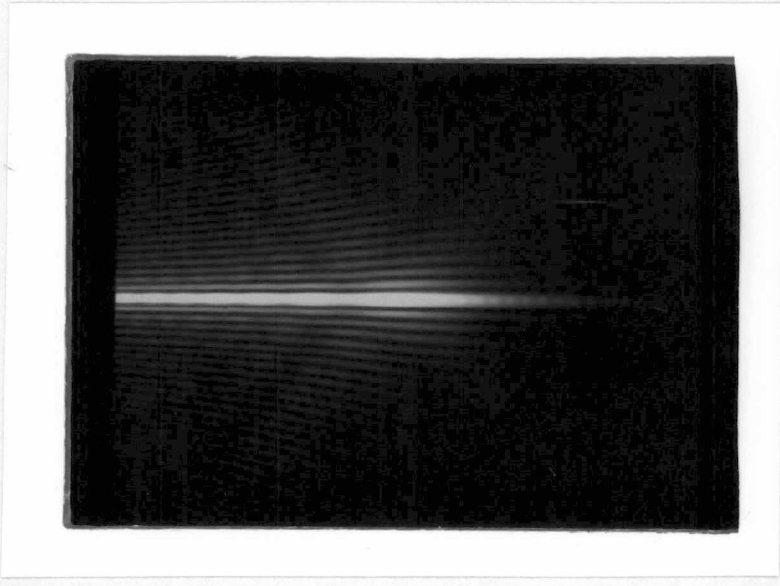

Fig. 21. Calculated meridional plane intensity corresponding to Fig. 20.

XI. CONCLUSIONS

A unified study, combining both theoretical and experimental analyses, has been made of the effects of aberrations on the intensity in the focal region resulting from a laser beam focused by a spherical surface lens. The close agreement between calculated and experimental results shows that the Fourier optics approach to the diffraction theory of aberrations produces a suitably accurate model of the behavior of focused laser radiation for practical optical systems.

The use of the thin lens approximation for modeling the effects of the focusing lens has been shown to be valid for the cases presented in this dissertation. The two computational techniques for calculating the propagation of the beam to focus, the convolution approach and the transform approach, have both proven useful. The computational efficiency of the transform approach, which leads to its use for calculating meridional plane intensity distributions, makes it the preferred method for analyzing focusing systems. Both of these methods readily lend themselves to vector-processing computational algorithms. Furthermore, the use of digital image processing equipment for calculation and data display has been shown to offer advantages in terms of ease of understanding and interpreting results.

While limitations to the approach were discussed in detail in Chapter VII, some of them bear repeating here. Polarization effects and propagation through inhomogeneous media were not considered, and a different approach is believed to be more fruitful for the inclusion of these phenomena. The thin lens approximation for modeling the lens effects produces results that differ from those of geometric ray tracing. Improvements to the thin lens assumption and resolving this discrepancy between scalar diffraction theory and geometric optics is clearly an area for further research.

The experimental analysis is a particularly important part of this work effort. The meridional plane intensity distribution images are the first known images of their kind, and thus represent a significant contribution to the diffraction theory of aberrations. The experimental technique itself also merits notice, and may be applied to specific focusing systems to study their performance.

The behavior of a focused laser beam is an important consideration in many applications, and will continue to increase in importance as the use of lasers for industrial and research purposes becomes more prevalent. The work presented here will hopefully provide insight into this problem, and contribute to its further study now and in the future.

BIBLIOGRAPHY

BIBLIOGRAPHY

[1] L. Rayleigh, *Phil. Mag.*, vol. 8, p. 403, May 1879.

[2] B. R. A. Nijboer, Ph.D. thesis, Dept. of Physics, Univ. of Groningen, 1942.

[3] F. Zernike, *Physica*, vol. 9, p. 974, 1942.

[4] F. Zernike and B. R. A. Nijboer, *La Théorie des Images Optique*, Paris: Revue d'Optique, 1949.

[5] R. Kingslake, *Proc. Phys. Soc.*, vol. 61, p. 147, 1948.

[6] K. Nienhuis, Ph.D. thesis, Dept. of Physics, Univ. of Groningen, 1948.

[7] K. Nienhuis and B. R. A. Nijboer, *Physica*, vol. 14, p. 590, 1948.

[8] A. Maréchal, *Rev. Opt.*, vol. 27, p. 73, 1948.

[9] E. H. Linfoot, *Recent Advances in Optics*, London: Oxford University Press, 1955.

[10] M. Born and E. Wolf, *Principles of Optics*, Oxford England: Pergamon Press, 1980.

[11] D. A. Holmes, J. E. Korka and P. V. Avizonis, "Parametric study of apertured focused Gaussian beams," *Appl. Opt.*, vol. 64, pp. 565-574, June 1972.

[12] A. J. Arimoto, "Aberration expansion and evaluation of the quasi-Gaussian beam by a set of orthogonal functions," *J. Opt. Soc. Am.*, vol. 64, pp. 850-856, June 1974.

[13] D. D. Lowenthal, "Maréchal intensity criteria modified for Gaussian beams," *Appl. Opt.*, vol. 13, pp. 2126-2133, Sept. 1974.

[14] E. J. Sklar, "Effects of small rotationally symmetrical aberrations on the irradiance spread function of a system with Gaussian apodization over the pupil," *J. Opt. Soc. Am.*, vol. 65, pp. 1520-1521, Dec. 1975.

[15] A. Yoshida, "Spherical aberration in beam optical systems," *Appl. Opt.*, vol. 21, pp. 1812-1816, Oct. 1982.

[16] J. M. Geary and P. Peterson, "Spherical aberration and diffraction derived via Fourier optics," *Opt. Eng.*, vol. 23, Jan. 1984.

[17] J. M. Geary and P. Peterson, "Intermediate spherical aberration," *Opt. Eng.*, vol. 25, pp. 1232-1240, Nov. 1986.

[18] Y. Li and E. Wolf, "Focal shifts in diffracted converging spherical waves," *Opt. Commun.*, vol. 39, pp. 211-215, Feb. 1981.

[19] Y. Li, "Dependence of the focal shift on Fresnel number and F number," *J. Opt. Soc. Am.*, vol. 72, pp. 770-774, June 1982.

[20] Y. Li and E. Wolf, "Three-dimensional intensity distribution near the focus in systems of different Fresnel numbers," *J. Opt. Soc. Am. A*, vol. 1, pp. 801-808, Aug. 1984.

[21] Y. Li, "Three-dimensional intensity distribution in low-Fresnel-number focusing systems," *J. Opt. Soc. Am. A*, vol. 4, pp. 1349-1353, Aug. 1987.

[22] J. W. Goodman, *Introduction to Fourier Optics*, San Francisco: McGraw-Hill, 1968.

[23] A. V. Oppenheim and R. W. Schafer, *Digital Signal Processing*, Englewood Cliffs, New Jersey: Prentice-Hall, 1975, pp. 105-115.

VITA

L. Montgomery Smith was born in Chattanooga, Tennessee, on March 28, 1956. After attending elementary and high schools in the area, he graduated from the McCallie School for Boys in 1974. He attended Rhodes College (formerly Southwestern at Memphis) from 1974 to 1978, graduating with a Bachelor of Science in Mathematics and Physics.

After working for Southern Research Institute in Birmingham, Alabama, and The Division of Radiological Health in Nashville, Tennessee, he attended The University of Tennessee at Knoxville, where he obtained a Bachelor of Science degree in Electrical Engineering in 1982. He came to The University of Tennessee Space Institute in 1982 on a graduate research assistantship and was awarded the Master of Science degree in Electrical Engineering in June 1984.

From 1984 to 1988 he worked as an engineer in the Center for Laser Applications at The University of Tennessee Space Institute in Tullahoma, Tennessee, where he also attended classes and performed his research for the Ph.D. degree. In December 1988, he was awarded the Doctor of Philosophy degree in Electrical Engineering from The University of Tennessee at Knoxville.